HHS Public Access

Author manuscript

Nat Neurosci. Author manuscript; available in PMC 2024 April 07.

Published in final edited form as:

Nat Neurosci. 2024 January ; 27(1): 63–77. doi:10.1038/s41593-023-01497-z.

Meningeal interleukin-17-producing T cells mediate cognitive impairment in a mouse model of salt-sensitive hypertension

Monica M. Santisteban[1,3,✉], **Samantha Schaeffer**[1], **Antoine Anfray**[1], **Giuseppe Faraco**[1], **David Brea**[1,4], **Gang Wang**[1], **Melissa J. Sobanko**[1], **Rose Sciortino**[1], **Gianfranco Racchumi**[1], **Ari Waisman**[2], **Laibaik Park**[1], **Josef Anrather**[1], **Costantino Iadecola**[1,✉]

[1]Feil Family Brain and Mind Research Institute, Weill Cornell Medicine, New York, NY, USA.

[2]Institute for Molecular Medicine, University Medical Center, Mainz, Germany.

[3]Present address: Department of Medicine, Vanderbilt University Medical Center, Nashville, TN, USA.

[4]Present address: Department of Neuroscience and Experimental Therapeutics, Instituto de Investigaciones Biomédicas de Barcelona, Barcelona, Spain.

Abstract

Hypertension (HTN), a disease afflicting over one billion individuals worldwide, is a leading cause of cognitive impairment, the mechanisms of which remain poorly understood. In the present study, in a mouse model of HTN, we find that the neurovascular and cognitive dysfunction depends on interleukin (IL)-17, a cytokine elevated in individuals with HTN. However, neither circulating IL-17 nor brain angiotensin signaling can account for the dysfunction. Rather, IL-17 produced by T cells in the dura mater is the mediator released in the cerebrospinal fluid and activating IL-17 receptors on border-associated macrophages (BAMs). Accordingly, depleting BAMs, deleting IL-17 receptor A in brain macrophages or suppressing meningeal T cells rescues cognitive function without attenuating blood pressure elevation, circulating IL-17 or brain angiotensin

✉**Correspondence and requests for materials** should be addressed to Monica M. Santisteban or Costantino Iadecola. monica.santisteban@vumc.org; coi2001@med.cornell.edu.

Author contributions

M.M.S, S.S., A.A., G.F., D.B.L. and R.S. conducted the experiments and performed the data analysis. G.W. performed the NO measurement of vessels ex vivo. M.J.S. performed the RNAscope experiments and assisted in mouse breeding and genotyping. G.R. performed the RT–qPCR. A.W. provided IL-17RA$^{flox/flox}$ mice and edited the manuscript. L.P., J.A. and C.I. supervised the research. M.M.S. and C.I. provided funding and wrote the manuscript.

Online content

Any methods, additional references, Nature Portfolio reporting summaries, source data, extended data, supplementary information, acknowledgements, peer review information; details of author contributions and competing interests; and statements of data and code availability are available at https://doi.org/10.1038/s41593-023-01497-z.

Reporting summary

Further information on research design is available in the Nature Portfolio Reporting Summary linked to this article.

Competing interests

C.I. is on the scientific advisory board of Broadview Ventures. All other authors declare no competing interests.

Extended data is available for this paper at https://doi.org/10.1038/s41593-023-01497-z.

Supplementary information The online version contains supplementary material available at https://doi.org/10.1038/s41593-023-01497-z.

signaling. Our data unveil a critical role of meningeal T cells and macrophage IL-17 signaling in the neurovascular and cognitive dysfunction in a mouse model of HTN.

HTN is a major cause of death and disability worldwide and a leading risk factor for dementia[1]. Although there have been notable advances in the pharmacotherapy, a sizable proportion of patients have uncontrolled or resistant HTN which is particularly damaging to the brain[2,3]. Furthermore, despite suggestive evidence that a rigorous control of blood pressure (BP) may lower the risk of mild cognitive impairment[4], the burden of HTN on the brain remains substantial, including a 10% risk of recurrent cerebrovascular events despite BP control and no proven strategy to prevent dementia[5]. Therefore, there is a need to gain a deeper understanding of the damaging effects of HTN on the brain and develop new approaches to protect cognitive health. Dysfunction of vital cerebrovascular regulatory mechanisms, such as the ability of neural activity to adjust the delivery of cerebral blood flow (CBF; functional hyperemia) or the regulation of microvascular perfusion by endothelial cells, has been strongly implicated in the deleterious effects of HTN on the brain[6]. However, the cellular and molecular basis through which the factors involved in BP elevation drive the neurovascular dysfunction associated with cognitive impairment remain poorly understood.

Salt sensitivity is a critical factor in essential HTN[7], affecting approximately 50% of individuals with HTN[8]. Experimental studies using the deoxycorticosterone acetate (DOCA)-salt model have provided evidence that the renin–angiotensin system (RAS) is activated in the brain and suppressed in the periphery[9,10]. Indeed, a large proportion of individuals with resistant HTN, particularly African–Americans and women, exhibit low levels of circulating renin, a key protease needed for angiotensin II (Ang II) production, suggesting suppression of systemic RAS[11,12]. It is also well established that HTN induces immune dysregulation and elevates circulating levels of the cytokine IL-17 in both animals and humans[13–15]. It is interesting that high dietary salt increases circulating levels of IL-17 by promoting polarization of helper T17 (T_H17) lymphocytes in the gut and induces neurovascular dysfunction and cognitive impairment[16,17]. However, the role of IL-17 in the deleterious effects of salt-sensitive HTN on cognitive function, its sources and targets, and its relationships with brain RAS, remain unexplored.

In the present study, we used the DOCA-salt model to examine the role of IL-17 in the neurovascular and cognitive dysfunction associated with salt-sensitive HTN. We found that DOCA-salt HTN alters key homeostatic mechanisms controlling the cerebral blood supply and leads to cognitive impairment. These deleterious effects are not driven by central Ang II signaling, but are associated with IL-17 signaling on both sides of the blood–brain barrier (BBB). In the circulation, IL-17 derived from gut and circulating T cells activates IL-17 receptor A (IL-17RA) on cerebral endothelial cells to impair their ability to regulate cerebral perfusion, but this mechanism does not explain in full the cognitive deficits. On the brain side, unexpectedly, IL-17 derived from T cells in the dura mater acts on IL-17RA on BAMs[18] to induce neurovascular uncoupling and cognitive impairment. Accordingly, depletion of meningeal T cells or BAMs completely rescues the cognitive phenotype. These findings unveil a previously unappreciated critical involvement of meningeal T cells and

IL-17 in the cognitive impairment associated with salt-sensitive HTN and suggest additional approaches to ameliorate the deleterious impact of HTN on cognitive function.

Results

IL-17 mediates neurovascular and cognitive impairment in DOCA-salt HTN

First, we sought to examine the impact of HTN on neurovascular and cognitive function. To this end, we used the DOCA-salt model of salt-sensitive HTN, in which mice are implanted with a subcutaneous pellet of DOCA and receive 0.9% NaCl in the drinking water[9,19]. DOCA-salt treatment evoked a sustained elevation of BP beginning 3 days after pellet implantation (Fig. 1a). An increase in circulating sodium was observed at 21 days (Supplementary Table 1), but the sodium content did not increase in the brain, kidney and small intestine (Extended Data Fig. 1a). However, as previously reported in mouse models and in individuals with refractory HTN[20], skin sodium content was increased without changes in potassium (Extended Data Fig. 1b). To examine the neurovascular effects of DOCA-salt HTN, we assessed CBF by laser–Doppler flowmetry in anesthetized mice with a cranial window overlying the somatosensory cortex under close monitoring of key physiological variables (Fig. 1b and Methods)[21,22]. DOCA-salt attenuated the increase in CBF evoked by neural activity induced by mechanical stimulation of the facial whiskers (functional hyperemia; Fig. 1b–d), as well as the increase in CBF produced by bathing the somatosensory cortex with acetylcholine (ACh; Fig. 1e), a response dependent on endothelial nitric oxide (NO)[23]. Both responses were impaired starting 10 days after DOCA. However, smooth muscle vasoactivity, tested by neocortical application of adenosine (Fig. 1f), BBB permeability to low-molecular-mass dextran (Extended Data Fig. 1c,d) and resting CBF (ml per 100 g min^{-1}) assessed by arterial spin label (ASL)–magnetic resonance imaging (MRI; Extended Data Fig. 1e,f) was not impaired 21 days after DOCA, indicating that the suppression of functional hyperemia and endothelial vasodilatation did not result from widespread neurovascular damage. DOCA-salt also altered cognitive function, as demonstrated by a reduction in the mice's ability to discriminate between familiar and novel objects (working memory) (Fig. 1g), a reduction of time spent in the target quadrant (TQ) during the Barnes maze probe trial (spatial learning and memory) (Fig. 1h) and impaired nest-building ability (activities of daily living) (Fig. 1i). Representative images from each group are shown for each of these cognitive tasks (Fig. 1g–i). Importantly, the neurovascular alterations preceded the development of cognitive impairment (Fig. 1d,e,g), an observation consistent with a mechanistic link between neurovascular dysfunction and cognitive impairment[24].

Based on the emerging role of IL-17 in human HTN[13–15,25,26] and in dietary salt-induced cognitive impairment[22], we then examined whether IL-17 contributes to the neurovascular and cognitive effects of DOCA-salt HTN. Circulating IL-17 increased gradually over the course of the DOCA-salt treatment (Fig. 2a), starting at day 10 when neurovascular dysfunction first became apparent (Fig. 1d,e). Focusing on the gut, an organ enriched with IL-17-producing cells[27], we observed that 21 d of DOCA-salt increased *Il17a* messenger RNA expression (Fig. 2b). To identify the cellular sources of IL-17, we induced DOCA-salt HTN in mice carrying the gene encoding enhanced green fluorescent protein (eGFP) at the

Il17a locus[28] and observed increased IL-17–GFP$^+$ cells at 21 d (Fig. 2c,d) in the small intestine lamina propria (LP), identified by flow cytometry to be T_H17 and γδT17 cells (Fig. 2e–g; Supplementary Fig. 1). T_H17 and γδT17 cells have been shown to enter the circulation[28,29] and they were also increased in blood and spleen in DOCA-salt (Fig. 2h,i), as in patients with HTN in whom circulating IL-17-producing cells are increased[25,26]. We found no evidence of IL-17 production by neutrophils (Extended Data Fig. 1g and Supplementary Fig. 2).

To test whether IL-17 contributes to the deleterious effects of salt-sensitive HTN, we induced DOCA-salt HTN in IL-17 deficient mice (IL-17 knockout (KO); Fig. 2j and Supplementary Table 2). IL-17KO mice developed an increase in BP and circulating sodium similar to WT mice (Extended Data Fig. 2a and Supplementary Table 1), but did not exhibit an attenuation in functional hyperemia and endothelial vasodilatation (Fig. 2k,l). Furthermore, no deficits were observed in either novel object recognition or Barnes maze tests (Fig. 2m,n). Thus, IL-17 produced by T_H17 and γδT17 cells is essential for neurovascular and cognitive dysfunction in DOCA-salt HTN.

IL-17 impairs endothelial vasodilatation by reducing NO

Next, we sought to identify the cellular targets of the IL-17 contributing to neurovascular and cognitive impairment. As endothelial cells are in direct contact with circulating IL-17, which is elevated in DOCA-salt HTN (Fig. 2a), we first assessed the contribution of cerebral endothelial IL-17RA. To this end, we deleted brain endothelial IL-17RA by administering a cerebral endothelial cell specific adeno-associated virus expressing Cre recombinase (AAV-BR1-iCre; intravenously (i.v.))[30,31] to IL-17RA$^{flox/flox}$ mice[32], referred to as IL-17RA^{bECKO}. AAV-BR1-iCre delivery in Ai14-ROSA^{tdTomato} reporter mice (Extended Data Fig. 3a) demonstrated widespread endothelial cell transduction in the cerebral microvasculature (Extended Data Fig. 3b). Most importantly, we observed 90–95% endothelial viral transduction in vessels <20 μm (Extended Data Fig. 3c,d), which include the arterioles involved in CBF regulation33. Then 3 weeks after AAV-BR1-iCre delivery in IL-17RA$^{flox/flox}$, we observed a reduction in *Il17ra* genomic DNA in sorted brain endothelial cells, but not in microglia (Extended Data Fig. 3e and Supplementary Fig. 3), consistent with the selectivity of this viral vector[31,34]. IL-17RA^{bECKO} mice (Fig. 3a) had increases in BP and circulating IL-17 comparable to those of DOCA-salt WT mice (Extended Data Fig. 2b and Supplementary Table 2), but the CBF response to ACh was completely rescued (Fig. 3b). However, no improvement was observed in functional hyperemia (Fig. 3c). As IL-17 has been shown to suppress endothelial NO production by inducing inhibitory endothelial nitric oxide synthase (eNOS) phosphorylation at Thr495 (ref. 22), we also examined NO production and eNOS phosphorylation in DOCA-salt treated mice. Resting and ACh-induced endothelial NO production was attenuated in DOCA cerebral microvascular preparations (Fig. 3d), an effect associated with an increase in eNOS inhibitory phosphorylation (Fig. 3e). However, as predicted by the rescue of endothelial vasoactivity (Fig. 3b), the increase in eNOS Thr495 phosphorylation was suppressed in IL-17RA^{bECKO} DOCA-salt mice (Fig. 3f), attesting to the link between endothelial IL-17RA and eNOS inhibitory phosphorylation. Consistent with the partial rescue in neurovascular

function, IL17RA^{bECKO} DOCA-salt mice displayed cognitive improvement only at novel object recognition, not the Barnes maze test (Fig. 3g,h).

BAMs contribute to the neurovascular and cognitive dysfunction in HTN

Cerebral endothelial IL-17RA knockdown ameliorated the neurovascular and cognitive function only partially, whereas total IL-17KO rescued the dysfunction in full, suggesting the involvement of IL-17RA on other vessel-associated cell types. BAMs, including perivascular and leptomeningeal macrophages, express IL-17RA[35] and have been implicated in models of neurovascular and cognitive dysfunction[21,36], raising the possibility that they may also play a role in DOCA-salt HTN. To test this hypothesis, we examined the effect of BAM depletion via intracerebroventricular delivery of liposome-encapsulated clodronate (Fig. 4a)[21,36]. Liposomes containing vehicle (phosphate-buffered saline (PBS)) or clodronate were injected intracerebroventricularly (i.c.v.) on the same day as DOCA-salt treatment was started. This protocol depleted 80% of perivascular and leptomeningeal BAMs (Fig. 4b,c) within the time-frame of the experiment[21], without affecting microglia or blood leukocytes[21], BBB permeability[31] or neurovascular function[21,36]. Dural macrophages were depleted initially but, unlike the leptomeningeal and perivascular BAMs, were fully restored within 21 d (Extended Data Fig. 4a,b). The BP (Extended Data Fig. 2c) and serum IL-17 (Supplementary Table 2) increases evoked by DOCA-salt were not affected by clodronate treatment. However, BAM depletion completely normalized functional hyperemia (Fig. 4d) and partially improved endothelial vasodilation (Fig. 4e). In addition, BAM depletion improved cognitive function as assessed by novel object recognition and the Barnes maze test (Fig. 4f,g). These observations demonstrate that BAMs contribute to the deleterious neurovascular and cognitive effects of DOCA-salt HTN.

IL-17RA-dependent ROS production in BAMs mediates the dysfunctions

Owing to their myeloid origin, BAMs are enriched with the reactive oxygen species (ROS)-producing enzyme Nox2 and are a major source of vascular oxidative stress[21,37,38]. Neocortical application of the ROS scavenger MnTBAP rescued the impairment of functional hyperemia in DOCA-salt (Fig. 4h), attesting to the involvement of ROS in the neurovascular dysfunction. Therefore, we sought to determine whether DOCA-salt increases ROS production in BAMs and, based on the results in IL-17KO mice (Fig. 2j–n), whether the effect is IL-17 dependent. Dissociated brain cells from WT control and DOCA-salt mice were incubated with the ROS probe dihydroethidium (Fig. 4i) and stained for identification of BAMs (CD45^{hi}CD11b^{+}CD36^{+}; Supplementary Fig. 4)[21,39], microglia (CD45^{int}CD11b^{+})[4,31] and endothelial cells (CD45^{-}Ly6C^{+})[31,40] using flow cytometry[21,31,39,40]. We found that DOCA-salt increased ROS production in BAMs, but not in microglia or endothelial cells (Fig. 4j). DOCA-salt failed to increase ROS in BAM of IL-17RA-deficient mice (Fig. 4k), indicating that IL-17 signaling is needed for BAM ROS production in DOCA-salt HTN. Consistent with this conclusion, recombinant IL-17 (10 ng ml^{-1}) increased ROS production in WT BAMs, as assessed with two different probes (Fig. 4l).

To provide further evidence that IL-17RA in BAMs is involved, we used a bone marrow (BM) chimera-based approach. We and others have demonstrated that BM transplantation

after total body irradiation repopulates leptomeningeal and perivascular compartments with BM-derived macrophages[21,31,41,42]. Therefore, we transplanted IL-17RA$^{-/-}$ or Nox2$^{-/-}$ BM into WT mice to replace BAMs with IL-17RA$^{-/-}$ or Nox2$^{-/-}$ BM-derived cells (Fig. 4m). After 3 months, mice were placed on the DOCA-salt protocol (Extended Data Fig. 2d,e). WT mice transplanted with WT BM (WT→WT) exhibited alterations in CBF responses and cognition identical to those observed in naive mice (Figs. 4n–q and 1d–h), indicating that, although BAMs in these mice are derived from the BM, they are pathogenically equivalent to native yolk sac-derived BAMs[21,36]. Deletion of either IL-17RA or Nox2 in BAMs prevented the impairment of functional hyperemia in full (Fig. 4n) and partially improved endothelial vasoactivity (Fig. 4o), as observed in the BAM depletion experiments (Fig. 4d,e). In addition, IL-17RA$^{-/-}$→ WT and Nox2$^{-/-}$→ WT chimeras showed improved cognitive function (Fig. 4p,q). Attesting to the requirement of IL-17RA in BAMs, ROS production was blunted in BAMs from IL-17RA$^{-/-}$→ WT DOCA-salt chimeras (Extended Data Fig. 4c). As ROS are a well-known product of IL-17 signaling[43] these data also provide evidence of IL-17RA activation in BAMs.

To complement the BM chimera data implicating IL-17RA in BAMs, we developed a new mouse expressing tamoxifen-inducible Cre recombinase under the control of the Mrc1 promoter (Mrc1$^{CreERT2/+}$; Fig. 5a). First, we sought to determine whether Mrc1^{CreERT2} heterozygosity altered BAM numbers and distribution across brain compartments (Extended Data Fig. 5a). To this end, after labeling BAM by injecting i.c.v. FITC–dextran (Extended Data Fig. 5b), we confirmed that the number of BAMs in dural, pial and perivascular spaces of Mrc1$^{CreERT2/+}$ mice were no different from those in Mrc1$^{+/+}$ (WT) mice (Extended Data Fig. 5c–g). Next, to characterize the efficiency of this new Cre driver mouse, we crossed Mrc1^{CreERT2} with Ai14 TdTM (Fig. 5b,c). After tamoxifen treatment, we found widespread TdTM expression in pial and perivascular BAMs (Extended Data Fig. 6a–f). TdTM was not detected in Iba1^{+} microglia (Extended Data Fig. 6e). Tamoxifen treatment of adult Mrc1$^{CreERT2/+}$ crossed with IL-17RA$^{flox/flox}$ (BAM$^{IL17RA-/-}$) led to a 78.9% reduction in IL-17RA+ BAMs (Fig. 5d,e and Extended Data Fig. 6g,h), without affecting the BP response (Fig. 5f) and circulating IL-17 elevation (Supplementary Table 2) induced by DOCA-salt. Consistent with the findings in IL-17RA$^{-/-}$→ WT chimeras, we observed full rescue of functional hyperemia without improvement of endothelial vasodilatation (Fig. 5g,h). In addition, BAM$^{IL17RA-/-}$ DOCA-salt mice showed improved cognitive function (Fig. 5i,j). Collectively, the findings with BM chimera and our new Mrc1$^{CreERT2/+}$ mouse provide converging evidence that IL-17RA in BAMs are critical for the alterations in functional hyperemia and cognitive function induced by DOCA-salt HTN.

HTN increases IL-17-producing T cells in the dura mater

Next, we sought to define the cellular source(s) of IL-17 acting on BAM IL-17RA to induce neurovascular and cognitive dysfunction. Recent evidence indicates that IL-17-producing T cells are present in the dura mater and able to modulate rodent behavior[44,45]. In agreement with these findings, *Il17a* mRNA was detected in the dura of control mice and was markedly increased by 21 d of DOCA-salt treatment (Fig. 6a). *Il17a* mRNA was not observed in brain tissue (Fig. 6a). To map IL-17-producing cells in brain and dura, we used IL-17–GFP reporter mice. Consistent with the mRNA data, IL-17–GFP^{+} cells were not observed in

the brain (Supplementary Fig. 5), but were found in the dura (Fig. 6b–d), as previously reported[44,46]. DOCA-salt treatment (21 d) led to a significant increase in IL-17–GFP$^+$ cells surrounding the venous sinuses but not in regions removed from the sinus (Fig. 6b,c). To determine whether these cells actually secrete IL-17, we performed an IL-17 ELISpot assay to detect cytokine release with single-cell resolution[47] in isolated dural leukocytes. We found that dural cells secrete IL-17 and this response is increased in DOCA-salt mice (Fig. 6e,f). We then used flow cytometry to characterize the IL-17–GFP$^+$ cells. We did not observe an increase in CD45$^+$ immune cells in the dura of DOCA-salt mice (Fig. 6g). We found no change in the total number of CD4 or T_H17 cells (Extended Data Fig. 7a,b), or the percentage of CD4-producing IL-17 (Fig. 6h), excluding a role for these cells. There was no change in the total number of total γδT cells (Extended Data Fig. 7c) and a trend toward an increase in the number of γδT17 cells (Extended Data Fig. 7d). Interestingly, we observed an increase in the percentage of γδT cells producing IL-17 (Fig. 6i). As the total number of γδT cells did not change (Extended Data Fig. 7c), changes in other cell populations would not impact the percentage of γδT cells producing IL-17. Therefore, consistent with data in the literature[44], we observed an increase in the proportion of dural γδT cells producing IL-17. The increase in dural IL-17 production after 21 d of DOCA-salt was associated with increased detection of IL-17 in the cerebrospinal fluid (CSF; Fig. 6j). To gain insight into how dura-derived IL-17 reaches the CSF, we assessed the structural integrity of the arachnoid barrier using immunohistochemistry for the arachnoid barrier tight junction marker claudin-11 (ref. 48). We found substancial tight junction remodeling in DOCA-salt mice, as evidenced by: (1) discontinuous tight junctions (Fig. 6k); (2) reduced arachnoid domain areas (Fig. 6l,m); and (3) altered tight junction morphology (Fig. 6k)[49,50]. Collectively, these findings suggest that IL-17 generated by T cells in the dura reaches the CSF in the subarachnoid space via a disrupted arachnoid barrier and engages IL-17RA on BAMs. Of note, we did not observe changes in key inflammatory genes (Extended Data Fig. 8a,b) or evidence of microglia and astrocyte activation (Extended Data Fig. 8c,d), suggesting that dura-derived IL-17 did not result in a massive neuroinflammatory reaction that could potentially contribute to cognitive impairment in DOCA-salt.

Dural γδT17 cells drive the cognitive impairment in HTN

Next, we sought to provide evidence in support of the involvement of dural IL-17-producing cells in the neurovascular and cognitive effects of DOCA-salt HTN. Dural γδT cells, like other γδT cells[51], are tissue resident, with only 1–2% being derived from the circulation under homeostasis[44]. However, in inflammatory conditions, an increased influx of γδT cells into lymph nodes and subsequent homing to inflamed tissues via the circulation has been shown[52,53]. Given that circulating T_H17 and γδT17 cells are both elevated in DOCA-salt, it is conceivable that T cells migrate from the circulation to the dura. To test this hypothesis, we utilized FTY720 (fingolimod), a sphingosine-1-phosphate receptor (S1PR) modulator that depletes circulating lymphocytes, including γδT17 and T_H17 cells, by preventing their egress from lymphoid tissues and gut, as well as other mechanisms[29,54–57]. FTY720 (1 mg kg^{-1} intraperitoneally (i.p.) every 3 d (ref. 22) was administered from day 7 to day 21 of DOCA-salt treatment (Fig. 7a) and did not affect the development of HTN (Fig. 7b). As expected, FTY720 significantly reduced circulating CD4$^+$ T cells (Fig. 7c) without affecting the elevation in circulating IL-17 in DOCA-salt mice (Fig. 7d). FTY720 depleted

IL-17–GFP^{+} cells in the dura (Fig. 7e), both T_H17 cells (Fig. 7f), and γδT17 cells (Fig. 7g). It is interesting that FTY720 did not ameliorate the CBF response evoked from the endothelium (Fig. 7h), attesting to its dependence on circulating IL-17 acting on cerebral endothelial IL-17RA and not BAMs. The reduction of IL-17-producing T cells in the dura was associated with full rescue of functional hyperemia (Fig. 7i) and improved cognitive function (Fig. 7j,k), as well as suppression of ROS production in BAMs (Extended Data Fig. 4d).

To confirm the role of dural γδT cells in the neurovascular and cognitive dysfunction in DOCA-salt, we infused anti-TCRγδ antibody into the cerebral ventricles (i.c.v.) using osmotic mini-pumps from day 7 to day 21 of DOCA-salt treatment (Fig. 7l) to deplete γδT cells in the dura (Fig. 7m). Delivery i.c.v. of this antibody has been previously shown to decrease γδT cell production of IL-17 in the dura[44], but did not affect the BP response to DOCA-salt (Fig. 7n). Consistent with results of the FTY720 experiments, γδT cell depletion in the dura did not improve endothelial vasodilatation (Fig. 7o). The reduction of γδT cells in the dura rescued functional hyperemia (Fig. 7p) and improved cognitive function (Fig. 7q,r). Thus, dural IL-17-producing T cells are the source of the IL-17 contributing to neurovascular and cognitive impairment in salt-sensitive HTN.

IL-17 is required for the cerebrovascular effects of Ang II

It is well established that DOCA-salt treatment leads to activation of the brain RAS[9,10], which has been implicated in endothelial dysfunction in large and small cerebral vessels[58]. In apparent contrast, our data suggest that IL-17 is essential for the neurovascular and cognitive dysfunction in DOCA-salt HTN. Therefore, we investigated the relationship between brain Ang II and IL-17 in this model. As expected, DOCA-salt treatment elevated Ang II levels in the brain and reduced it in the circulation (Fig. 8a,b). These effects were associated with mRNA upregulation of brain Ang II receptors type 1A (AT1R) (*Agtr1a*; Fig. 8c) and downregulation of kidney renin (*Ren1*; Fig. 8d), confirming activation of the RAS in the brain and suppression in the periphery[58]. Central AT1R blockade by infusion i.c.v. of losartan (Fig. 8e) prevented the increase in BP caused by DOCA-salt[9] (Extended Data Fig. 2f), but did not attenuate the increase in circulating IL-17 (Supplementary Table 2). Accordingly, chronic losartan i.c.v. restored functional hyperemia (Fig. 8f), but did not improve endothelium-dependent vasodilatation (Fig. 8g), consistent with circulating IL-17 being the predominant mediator of the endothelial dysfunction. Central AT1R blockade ameliorated cognitive impairment only partially, with an improvement observed only in novel object recognition, but not at the Barnes maze test (Fig. 8h,i). As Ang II induces ROS production in BAMs leading to neurovascular dysfunction[21], we wondered whether IL-17 signaling in BAMs is required for Ang II-induced ROS production. Ang II stimulation increased ROS production in WT but not IL-17RA$^{-/-}$ BAMs (Fig. 8j). However, indices of brain RAS activation were not attenuated in IL-17KO mice (Extended Data Fig. 9a) or mice in which dural production of IL-17 was suppressed by treatment with FTY720 (Extended Data Fig. 9b), suggesting that brain RAS activation in the absence of dural IL-17 is not sufficient to induce neurovascular dysfunction. In support of this conclusion, bathing the cerebral cortex with Ang II to activate AT1R on BAMs[21] induced neurovascular dysfunction in WT but not IL-17KO mice (Fig. 8k,l). Thus, IL-17 signaling is necessary for

the contribution of Ang II to the neurovascular and cognitive impairment of salt-sensitive HTN.

Discussion

We have demonstrated that the neurovascular and cognitive dysfunction associated with salt-sensitive HTN is mediated by two distinct mechanisms involving IL-17 signaling in cerebral endothelium and BAMs (Extended Data Fig. 10): (1) in the circulation, IL-17 produced by T cells acts on cerebral endothelial IL-17RA to reduce NO production, leading to suppression of endothelial vasodilation without affecting the increase in CBF induced by neural activity; and (2) in the brain, IL-17 produced by dura T cells acts on IL-17RA on BAMs to induce vascular oxidative stress and suppression of functional hyperemia with minimal effects on endothelial function. However, these two mechanisms do not contribute equally to the cognitive dysfunction: counteracting the effect of circulating IL-17 by endothelial IL-17RA deletion rescues cognition only partially, whereas counteracting the sources (T cells) or targets of central IL-17 (BAMs or BAM IL-17RA) rescues cognitive function in full. Furthermore, eNOS phosphorylation is not involved in the mechanisms of neurovascular coupling because functional hyperemia can be rescued completely by BAM depletion or IL-17RA deletion in BAMs despite persistent endothelial dysfunction. Thus, the deleterious effects of BAMs on functional hyperemia cannot be attributed to endothelial dysfunction or eNOS phosphorylation. Therefore, the data unveil an unanticipated central role of meningeal T cells in the deleterious cognitive effect of salt-sensitive HTN.

There is increasing evidence that inflammation and immunity participate in the pathobiology of HTN[59]. Pioneering studies have unveiled a role of innate and adaptive immunity in the central and peripheral mechanisms driving the elevation in BP and on the end-organ damage, particularly in the kidney and the vasculature[60,61]. In this context, T cells and IL-17 have emerged as important mediators of the effect of Ang II and DOCA-salt HTN on peripheral organs and vessels, in part verified in patients with hypertension[62]. In the present study, we extend these observations by providing evidence that dural T cells and IL-17 play a critical role in the neurovascular and cognitive deficits in a model of HTN reproducing key attributes of the human disease[10]. Although the dura mater has recently been recognized as a major player in the immune responses of the brain underlying brain injury and repair[44,63], our findings provide insight into a previously unrecognized pathogenic role of meningeal immunity in HTN. Our studies revealed that the dura is the critical site of the immune responses underlying the neurovascular and cognitive deficits in HTN. This process is driven by a crosstalk between dural T cells and BAMs through IL-17 signaling. Thus, depletion of IL-17-producing T cells in the dura, depletion of BAMs or deletion of IL-17RA on BAMs rescues the cognitive deficits in full. As for the mechanisms by which BAMs alter neurovascular coupling, evidence from our previous studies implicate Ang II[21] and amyloid-β[36] inducing BAM production of ROS, which are thought to inactivate neuronal NO and other vasoactive mediators released from neurons and converging on resistance arterioles to mediate vasodilation[33].

The DOCA-salt model is associated with increases in brain RAS signaling and reduction of the systemic RAS[10], which we have verified by central and peripheral measurements of Ang

II. DOCA-salt HTN is well established as inducing alterations in cerebral vascular regulation both in vivo and in isolated cerebral arteries and arterioles[19,58]. Surprisingly, however, our study showed that the vascular effects of Ang II, mediated by ROS production by BAMs, require IL-17. Thus, ex vivo Ang II is unable to increase ROS production in BAMs in the absence of IL-17RA, and in vivo Ang II applied to the neocortex to target leptomeningeal and perivascular BAMs does not induce neurovascular dysfunction in IL-17KO mice. These observations unveil a critical requirement of IL-17 in the deleterious effects of Ang II. Considering the key role that Ang II and IL-17 signaling play in health and disease, the molecular basis of their interaction is of great interest and will require further exploration.

Owing to the absolute reliance of the brain on the delivery of blood flow, reduced cerebral perfusion or alterations in neurovascular regulation have long been implicated in cognitive impairment induced by vascular factors as well as Alzheimer's disease[64,65]. Our studies, in general, support a link between CBF regulation and cognitive health, but they also suggest effects of IL-17 independent of blood flow. Although resting CBF is not reduced, blocking cerebral endothelial IL-17 signaling rescues endothelial vasoactivity and produces partial cognitive improvement. On the other hand, counteracting central Ang II signaling rescues only neurovascular coupling and leads to a partial improvement in cognition. Although it is conceivable that endothelial dysfunction and neurovascular uncoupling could play an additive role in the cognitive deficits, this possibility seems unlikely because depletion of dural T cells provides complete cognitive rescue while improving only neurovascular coupling and not endothelial function. Direct effects of IL-17 on neurons have been demonstrated in other models[44,45,66], which, together with the vascular effects, could contribute to the cognitive dysfunction.

It is well established that HTN is a leading risk factor for cognitive impairment caused by both vascular factors and neurodegeneration[6], but the evidence that antihypertensive therapy reduces such a risk is inconsistent and limited[67,68]. Our findings reveal an additional layer of complexity in the deleterious effects of HTN on the brain. The central actions of Ang II are critical for the development of HTN by inducing neurohumoral dysfunction. This aspect was highlighted by our observation that central inhibition of AT1R prevented BP elevation completely but did not rescue the cognitive dysfunction in full. Although BP control remains critical for attenuating hypertensive end-organ damage to kidney, heart and vasculature[69], full protection of the brain may also require targeting meningeal immunity. Considering the diversity of mechanisms underlying human HTN[70], efforts to select patients with HTN in which immune factors are involved may identify individuals at greater risk for the deleterious effects of dural immune signaling on the brain. As the infectious complications of suppressing immune signaling is a well-known concern in patients with cardiovascular diseases[71], strategies to selectively target dural immunity would be required[72].

Methods

Details on antibodies used and specific primer sequences are found in the Online Supplement.

Experimental mouse models

All procedures were approved by the Institutional Animal Care and Use Committee of Weill Cornell Medicine and performed in accordance with the National Institutes of Health Guide for the Care and Use of Laboratory Animals. All studies were performed in a blinded fashion in male mice aged 3–5 months. Mice were group housed in a specific pathogen-free facility (22 °C, 45–65% humidity and 12 h light:dark cycle), with free access to food and water. Strains used are: C57BL/6 mice (WT, weight 25–30 g; JAX, Jackson Laboratory), IL-17–GFP reporter mice (C57BL/6-*IL17a*^{tm1Bcgen}/J, JAX strain no. 018472), IL-17KO mice (*IL17a*$^{tm1.1(icre)Stck}$/J, JAX strain no. 016879) and IL-17RA$^{flox/flox}$ mice[32]. IL-17RA$^{flox/flox}$ mice were crossed with the germ-cell-driven Sox2-Cre mice (B6.Cg-*Edil3*$^{Tg(Sox2-cre)1Amc}$/J, JAX strain no. 008454)[73] to generate whole-body IL-17RA KO mice. BM chimera experiments detailed below were performed on C57BL/6 mice receiving donor cells from IL-17RA KO mice or B6.129S-*Cybb*^{tm1Din}/J mice (*Nox2*$^{-/-}$, JAX strain no. 002365), both lines being congenic for C57BL/6. AAV-BR1-iCre experiments detailed below were performed on B6.Cg-*Gt(ROSA)26Sor*$^{tm14(CAG-tdTomato)Hze}$/J (Ai14 TdTomato reporter, JAX strain no. 007914) and homozygous IL-17RA$^{flox/flox}$ mice. Mrc1^{CreERT2} mice were generated by Cyagen. The Mrc1-targeting construct was linearized by restriction digestion with NotI, followed by phenol–chloroform extraction and ethanol precipitation. The linearized vector was transfected into C57BL/6 ES cells according to Cyagen's standard electroporation procedures. The transfected ES cells were subject to G418 selection (200 μg ml^{-1}) 24 h post-electroporation. Then, 179 G418-resistant clones were picked and amplified in 96-well plates. Two copies of 96-well plates were made, one copy was frozen and stored at −80 °C and the other was used for DNA isolation and subsequent PCR screening for homologous recombination. The PCR screening identified 18 potential targeted clones, from among which 6 were expanded and further characterized by Southern blotting analysis. Five of the six expanded clones were confirmed to be correctly targeted.

The *Mrc1* gene (National Center for Biotechnology Information reference sequence: NM_008625.2) is located on mouse chromosome 2. Some 30 exons have been identified with the ATG start codon in exon 1 and the TAG stop codon in exon 30. In the targeting vector, the coding region of exon 1 plus part of intron 1 was replaced with the CreERT2-poly(A) cassette. Correct integration of the CreERT2-poly(A) cassette was confirmed by diagnostic PCR. Sequencing of the genomic region of interest after amplification by PCR was further used to verify correct integration. After germline transmission, correctly targeted founders were crossed with C57BL/6J mice to establish the colonies for the present study. Adult 6- to 10-week-old mice were treated with tamoxifen citrate (Sigma-Aldrich, catalog no. T-5648; oral gavage; 200 mg kg^{-1}) once a day for 5 d consecutively. Female mice were not included in the present study, because previous studies have shown that they have a blunted hypertensive and immune response to DOCA-salt[74].

DOCA-salt HTN

Mice were randomized to treatment group and anesthetized by isoflurane inhalation for subcutaneous implantation of a 50-mg pellet of DOCA (Innovative Research of America, catalog no. M-121) or sham surgery of equal duration[19]. After recovery from anesthesia, DOCA animals were maintained on standard chow and free access to 0.9% NaCl in

autoclaved tap water. Control animals were maintained on standard chow and free access to autoclaved tap water. Systolic blood pressure (SBP) was monitored in awake mice using tail-cuff plethysmography (Hatteras, Multi-channel blood pressure analysis software, catalog no. MC4000)[21,31]. Mice were acclimated to tail-cuff plethysmography for 1 week before pellet or sham surgery, and SBP was monitored twice a week after initiation of DOCA-salt.

Tissue sodium measurement

Mice were anesthetized with isoflurane and blood was collected through cardiac puncture. Brain, kidney, skin (dorsal abdomen) and distal small intestine (distal 10 cm) were isolated, flash frozen and stored at −80 °C until analysis. After 15 min, blood was centrifuged at 2,000*g* for 15 min and serum was separated and stored at −80 °C until analysis. The serum renal chemical panel was performed by the Laboratory of Comparative Pathology of Weill Cornell Medicine Research Animal Resource Center, and the tissue mineral panel for sodium measurement was performed by the Animal Health Diagnostic Center Toxicology Lab of Cornell University Veterinary Medicine using inductively coupled plasma–atomic emission spectrometry (ICP–AES)[75,76].

General surgical procedures for CBF studies

Mice were anesthetized with isoflurane (induction, 5%; maintenance, 2%) and artificially ventilated with a mixture of N_2 and O_2. One of the femoral arteries was cannulated for recording mean arterial pressure (MAP) and collecting blood samples. Rectal temperature was maintained at 37 °C. After surgery, isoflurane was discontinued and anesthesia was maintained with urethane (750 mg kg^{-1}, i.p.) and chloralose (50 mg kg^{-1}, i.p.). Throughout the experiment, the level of anesthesia was monitored by testing motor responses to tail pinch. Arterial blood gases were monitored at the start and end of the experiment and maintained at partial O_2 pressure (PO_2) of 100–110 mmHg, partial CO_2 pressure (PCO_2) of 30–40 mmHg and pH 7.3–7.4 (ref. 21). As in previous studies[77], MAP remained within the autoregulated range for CBF (control, 82.77 ± 0.85 mmHg; DOCA, 106.37 ± 0.99 mmHg; $P < 0.05$). Owing to the anesthesia, the baseline BP and the increase in BP induced by DOCA-salt was lower than that observed in awake mice[9].

Experimental protocol for experiments monitoring CBF reactivity

As previously described[21,22,36], a small craniotomy (2 × 2 mm^2) was performed to expose the parietal cortex, the dura was removed and the site was superfused with Ringer's solution (37 °C and pH 7.3–7.4)[21]. CBF was continuously monitored at the site of superfusion with a laser–Doppler flow probe (Perimed) positioned stereotaxically on the cortical surface and connected to a data acquisition system (PowerLab, LabChart). CBF values were expressed as percentage increases relative to the resting level. After MAP and blood gases were stable, CBF responses were recorded. The whisker-barrel cortex was activated for 60 s by stroking of the contralateral vibrissae and the evoked changes in CBF were recorded. ACh (10 μM; Sigma-Aldrich) or adenosine (400 μM; Sigma-Aldrich) was superfused on the exposed neocortex for 5 min[21,22,36]. In some experiments, CBF responses were tested before and after 30 min of superfusion with the ROS scavenger MnTBAP (100 μM)[21,77] or Ang II (500 nM)[21].

BBB permeability

BBB permeability was assessed using fluorescein–dextran (FITC–dextran, M_r = 3 kDa; 100 µl of 1% solution i.v.), as previously described[21,31]. The tracer was allowed to circulate for 20 min and then mice were transcardially perfused with cold PBS to clear the intravascular tracer. Brains were removed and the olfactory bulb, brainstem and cerebellum were discarded. Samples were weighed and frozen on dry ice and stored at −80 °C until analysis. Tissue was homogenized in 400 µl of PBS, mixed with 400 µl of methanol and centrifuged at 13,000*g* for 30 min. The supernatant was used for measurement of the amount of FITC–dextran (485-nm excitation and 530-nm emission), measured in duplicate using a fluorescence spectrophotometer, together with standards, and normalized to brain tissue weight.

Measurement of resting CBF by ASL–MRI

CBF was assessed quantitatively using ASL–MRI at 21 d of DOCA-salt, performed on a 7.0-T 70/30 Bruker Biospec small-animal MRI system with 450 mT m^{-1} gradient amplitude and a 4,500 T m^{-1} s^{-1} slew rate. A volume coil was used for transmission and a surface coil for reception. Anatomical localizer images were acquired to find the transversal slice approximately corresponding to bregma +0.5 mm. This position was used for subsequent ASL–MRI, which was based on a flow-sensitive, alternating, inversion recovery, rapid acquisition with relaxation enhancement (FAIR-RARE) pulse sequence labeling the inflowing blood by global inversion of the equilibrium magnetization. One axial slice was acquired with a field of view of 15 × 15 mm^2, spatial resolution of 0.117 × 0.117 × 1 mm^3, TE (echo time) of 5.368 ms, effective TE of 48.32 ms, recovery time of 10 s and a RARE (rapid imaging with refocused echoes) factor of 72. Some 22 turbo inversion recovery values ranging from 30 ms to 2,300 ms were used and the inversion slab thickness was 4 mm. For computation of resting CBF (rCBF), the Bruker ASL perfusion-processing macro was used, which uses a published model[78] and includes steps to mask out the background. The masked rCBF images were exported to Analyze format on the MRI console. The ASL images were analyzed by ImageJ and the average CBF value is reported in milliliters per 100 grams of tissue per minute[22].

Novel object recognition test

The novel object recognition test task was conducted in a plastic box measuring 29 cm × 47 cm × 30 cm high[21,22]. Stimuli consisted of plastic objects that varied in color and shape, but had a similar size. A video camera was used to record the testing session for offline analysis using AnyMaze software. Mice were acclimated to the testing room for 1 h each day before the start of each day. On day 1, mice were acclimated to the testing chamber (habituation). On day 2, mice were placed in the same chamber in the presence of two identical sample objects and were allowed to explore for 5 min. After an intersession interval of 1 h, mice were placed in the same chamber, but one of the two objects was replaced by a novel object. Mice were allowed to explore for 5 min. Between trials, the maze was cleaned with 10% ethanol in water to minimize olfactory cues. Exploratory behavior was assessed manually by two experimenters blinded to the treatment group. Exploration of an object was defined as the mouse sniffing the object or touching the object while looking at it[21]. A minimal

exploration time for both objects (total exploration time) during the test phase (5 s) was used. The amount of time taken to explore the novel object was expressed as a percentage of the total exploration time and provided an index of working memory.

Barnes maze test

As described previously[21,22], we used a Barnes maze consisting of a circular open surface (90 cm in diameter) elevated to 90 cm by four wooden legs. There were 20 circular holes (5 cm in diameter) equally spaced around the perimeter, positioned 2.5 cm from the edge of the maze. No wall or intra-maze visual cues were placed around the edge. A plastic escape box ($11 \times 6 \times 5$ cm^3) was positioned beneath one of the holes. Mouse movement was tracked with the AnyMaze software (Stoelting). Mice were tested in groups of ten and between trials were placed into cages in a dark room adjacent to the test room for the intertrial interval (45 min). Mice were habituated to the dark room for 60 min before the start of each day. No habituation trial was performed. The acquisition phase consisted of three consecutive training days with three 3-min trials per day with the escape hole located at the same location across trials and days. On each trial, a mouse was placed into a start tube located in the center of the maze, the start tube was raised and the buzzer was turned on until the mouse entered the escape hole. After each trial, mice remained in the escape box for 60 s before being returned to their home cage. Between trials, the maze was cleaned with 10% ethanol in water to minimize olfactory cues. Three parameters of learning performance were recorded: (1) latency to locate the escape hole, (2) distance traveled before locating the escape hole and (3) number of errors made. Errors were defined as head-pokes into nonescape holes and were counted manually. On the fourth day, the probe trial was performed and consisted of a 1.5-min trial where the escape hole had been removed. The memory parameter recorded was a percentage of time spent in the TQ where the escape hole used to be.

Nest building

The ability of mice to build nests was assessed by the Deacon rating scale[22,79]; 1 h before the dark cycle, each mouse was placed in a new clean cage containing 5 g of nestlet (Ancare) in the middle of the cage. Food, water and lighting parameters were not changed from standard housing practices. The next day, nests were assessed on a rating scale of 1–5 (ref. 79) and untorn nestlet pieces were weighed. The cognitive parameters recorded were (1) nest score and (2) percentage of untorn nestlet.

IL-17 measurement

IL-17 concentration in serum was measured by either cytometric bead array mouse IL-17A Enhanced Sensitivity Flex Set (BD Biosciences)[22] or electrochemiluminescence-based multi-array MSD V-Plex Mouse IL-17A Kit (MesoScale)[80], according to the manufacturer's instructions.

Immunofluorescence

IL-17–eGFP and WT mice were anesthetized with sodium pentobarbital (120 mg kg^{-1}, i.p.) and perfused transcardially with PBS followed by 4% paraformaldehyde (PFA) in

PBS. Distal small intestine, brain and skull cap were removed and post-fixed overnight in 4% PFA. Small intestine was then submerged in 30% sucrose solution for 3 d, frozen and sections (thickness 30 μm) were cut through the whole distal small intestine using a cryostat and then placed on a slide. Free-floating coronal brain sections (thickness 40 μm) were cut through the whole brain using a vibrating microtome. Dura whole mounts were prepared by careful stripping from the skull cap using fine surgical forceps, as has been previously described by us[22,28,81] and others[44,46,82]. For leptomeningeal mounting, PFA-perfused brains were post-fixed in methanol on a shaker at room temperature for 10 min[48]. Then, the leptomeninges was carefully stripped from the surface of the brain and mounted on slides for staining[48–50]. Brain sections and dura whole mounts were permeabilized in 0.5% Triton–PBS and then blocked with 5% normal donkey or goat serum in 0.1% Triton–PBS. Sections were incubated with primary antibodies (Supplementary Table 3) at 4 °C overnight in 2% normal donkey or goat serum in 0.1% Triton–PBS. Leptomeningeal mounts were blocked with 5% normal donkey or goat serum and 5% bovine serum albumin in 0.1% Triton–PBS. Sections were then incubated with species-specific secondary antibody (1:100, Jackson ImmunoResearch whole immunoglobulin (Ig)G affinity-purified antibodies) and mounted on slides with VectaShield Hardset mounting medium with DAPI (Vector Labs), visualized with a laser-scanning confocal microscope (Leica TCS SP8, Leica Application Suite X) and analyzed on ImageJ software by an investigator blinded to the treatment groups. IL-17–GFP cells in the dura were analyzed as sinus associated if they were in close proximity to the venous sinus, and nonsinus if they were in all other areas of the dura. For $TdTM^+$ vessel quantification in AAV-BR1-Cre-injected Ai14 TdTM reporter mice, 110 vessels were randomly selected from 10 different images of the cortex of 5 mice. The area of TdTM as a percentage of CD31 immunofluorescence was quantified.

Cell suspension preparation from lymph nodes, spleen and blood

At the indicated timepoints, mesenteric, axillary and inguinal (nonbrain draining) lymph nodes were extracted from each animal and pooled, placed on a premoistened 70-μm cell strainer, gently triturated, washed with 10 ml of PBS and spun at 500*g* for 7 min (ref. 22). The cell suspension was then either stained for flow cytometry analysis or processed for analysis of intracellular cytokines. The spleen was removed, its epithelium was cut longitudinally and cells were isolated as described for the lymph nodes. Blood (150 μl) was drained from the submandibular venous plexus into heparinized tubes, incubated with erythrocyte lysis buffer and spun at 500*g* for 7 min, and cells were stained for flow cytometry analysis[22].

Isolation of intestinal LPMCs

Mice were euthanized by isoflurane overdose and the small intestines were removed and separated as previously described[22,28]. Peyer patches were cut out from the small intestine and the small intestines were completely cleaned of mesenteric fat and intestinal contents[22]. Then intestines were opened longitudinally, washed of fecal contents with PBS, cut into approximately 1-cm pieces and placed into 20 ml of Hanks' balanced salt solution (HBSS)/10 mM Hepes, 8% fetal bovine serum (FBS), 4 mM EDTA and 0.5 mM dithiothreitol. Next intestinal pieces were washed 3× in a shaking incubator set at 250 r.p.m. and 37 °C for 20 min. After each round, intestinal pieces were vortexed for 20 s and the cell

suspension containing intraepithelial lymphocytes (IELs) was collected. Suspensions from the three washes of IELs were combined and filtered over 0.3 g of prewashed nylon wool placed into a 10-ml syringe and then over a 70-μm strainer. Intestinal pieces were washed with complete PBS to remove EDTA, minced thoroughly with scissors and placed into 5 ml of 0.2 mg ml^{-1} of collagenase D in HBSS/10 mM Hepes with 5% FBS. Then the intestinal pieces were digested at 250 r.p.m. and 37 °C for 20 min, followed by 20 s of vortex. The resulting cell suspension contained the LP mononuclear cells (LPMCs) and was filtered with a 40-μm nylon cell strainer; the strainer was washed with 10 ml of PBS. LPMC cell suspensions were spun at 500*g* for 10 min at 4 °C. Cell pellets were resuspended in 8 ml of 44% Percoll and overlaid on 5 ml of 67% Percoll. Gradients were centrifuged at 500*g* for 20 min at 4 °C (with break off) and cells at the interface were collected and washed with 10 ml of PBS. Cells were then spun at 500*g* for 10 min at 4 °C and stained for flow cytometry analysis.

Flow cytometry and FACS

For surface marker analysis, approximately 1×10^6 cells were resuspended in 50 μl of FACS buffer. Cells were blocked with anti-CD16/CD32 for 10 min at 4 °C and then stained with the appropriate antibodies for 15 min at 4 °C. The antibodies and concentrations used are listed in Supplementary Table 4. Cells were washed with FACS buffer, resuspended in 200 μl of FACS buffer and acquired NovoSampler Q (NovoCyte Quanteon, NovoExpress) and absolute cell numbers and frequencies were recorded. Samples were analyzed with FlowJo (v.10, Tree Star) by an investigator blinded to the treatment groups (Supplementary Figs. 1–4). Appropriate isotype controls, ‘fluorescence minus one’ staining and staining of negative populations were used to establish sorting parameters. Endothelial cells were identified as $CD45^{-}Ly6C^{+}$ and microglia as $CD45^{int}CD11b^{+}$ (ref. 31). Brain macrophages were identified as $CD45^{hi}CD11b^{+}CD36^{+}$ (refs. 24,39,83–85). We could not use the canonical BAM marker CD206 because this approach requires cell permeabilization for intracellular antibody access and cannot be used together with live cell assays, such as those for measuring ROS production. Therefore, we used CD36 as a marker of BAMs, as shown by single-cell RNA sequencing data[35]. To validate this approach, we quantified the overlap of CD206 and CD36 expression within the CD45 and CD11b population. We found that close to 90% of CD206 cells express CD36 (Supplementary Fig. 4b), attesting to the validity of this approach. For FACS, endothelial and microglia cells (Supplementary Fig. 3) were sorted on a FACSAria II (BD Biosciences) or CytoFlex SRT (Beckman) and collected in sample buffer for genomic DNA reverse transcription quantitative PCR (RT–qPCR).

Cerebral endothelial knockdown of IL-17RA

Seven- to ten-week-old C57BL/6J, B6.Cg-*Gt(ROSA)26Sor*$^{tm14(CAG-tdTomato)Hze}$/J (Ai14 TdTomato reporter, stock no. 007909) and IL-17RA$^{flox/flox}$ mice[32] were administered 1.8×10^{11} viral genomes (VG) in 100 μl of sterile PBS with AAV-BR1-iCre[30,31] (AAV-NRGTEWD-CAG-iCre). In Ai14 TdTomato mice, virus transduction was assessed by immunofluorescence and analyzed as TdTomato colocalization with the endothelial CD31 marker (100 vessels per mouse; $n = 3$ mice). In IL-17RA$^{flox/flox}$ mice, DOCA pellets were implanted 3 weeks after AAV-BR1-iCre administration.

NO measurement in pial microvessels

Pial microvessels were removed under a dissecting microscope[86] and incubated with DAF-FM (25 μM; Molecular Probes) in artificial CSF (124 mM NaCl, 26 mM $NaHCO_3$, 5 mM KCl, 1 mM NaH_2PO_4, 2 mM $CaCl_2$, 2 mM $MgSO_4$, 20 mM glucose, 4.5 mM lactic acid, oxygenated with 95% O_2 and 5% CO_2, pH 7.4) at room temperature for 45 min[22,86]. Time-resolved fluorescence was measured every 60 s with an exposure time of 150 ms using image analysis software (IPLab, Scanalytics Inc). After a stable fluorescence baseline had been achieved, microvessels were superfused with ACh (100 μM) for 15 min. DAF-FM fluorescence intensity is expressed as relative fluorescence units (r.f.u.) μm^{-2}, where μm^2 is unit of the area in which relative fluorescence was measured.

Western blotting

Cerebral blood vessel samples were lysed in radioimmunoprecipitation assay (RIPA) buffer (50 mM Tris-HCl, pH 8.0, 150 mM NaCl, 0.5% deoxycholic acid, 0.1% sodium dodecylsulfate (SDS), 1 mM EDTA, pH 8.0, 1% IGEPAL CA-630) and equal volumes were mixed with SDS sample buffer, boiled and analyzed on 4–12% SDS polyacrylamide gels. Proteins were transferred to poly(vinylidene) membranes (Millipore), blocked with 5% milk in Tris-buffered saline (TBS)/0.1% Tween-20 (TBS-T) and incubated with anti-phospho-eNOS (Thr495) and anti-eNOS (Supplementary Table 3; 1:1,000, Cell Signaling, catalog nos. 9574 and 9572, respectively). Membranes were washed in TBS-T, incubated with goat anti-rabbit secondary antibodies conjugated to horseradish peroxidase (HRP; 1:5,000; Jackson ImmunoResearch peroxidase affinity-purified whole IgG antibodies), and protein bands were visualized with Clarity Western ECL Substrate (BioRad) on a BioRad ChemiDoc MP Imaging System. Data were analyzed in ImageLab. Raw images and molecular mass marker annotations are provided in Supplementary Figs. 6–13.

In vivo treatments

To deplete $CD206^+$ brain macrophages, clodronate- or PBS-loaded liposomes were prepared as previously described[21,31]. Under isoflurane anesthesia, 10 μl of clodronate liposomes (5 mg ml^{-1}) and PBS liposomes (vehicle) were injected (rate, 500 nl min^{-1}, approaching CSF clearance rates of 300–400 nl min^{-1} (ref. 87)) into the cerebral ventricles (i.c.v.) with a Hamilton syringe through a burr hole drilled on the right parietal bone (coordinates: 0.5 mm posterior to bregma, 1.0 mm lateral from midline, 2.3 mm below the brain surface) on the same day as DOCA-pellet implantation. Assessments were made 21 d after the injection, allowing ample time for any potential perturbations in CSF homeostasis to subside. Attesting to the lack of untoward effects of the injection, we did not observe any alterations in cerebrovascular regulation (functional hyperemia, endothelial vasoactivity, smooth muscle vasomotor function), BBB permeability or cognition in mice injected with the same volume of control PBS liposomes. FTY720 (1 mg kg^{-1}; Cayman Chemical)[22] was injected i.p. 3× every 3 d after the first week of DOCA-salt. Control and DOCA-salt mice were equipped with an i.c.v. cannula attached to a osmotic mini-pump (ALZET brain infusion kit 3, no. 0008851, pump no. 1004) for delivery of anti-TCRγδ antibody (UC7-13D5, BioXCell 0.1 μg h^{-1}) or isotype control (polyclonal Armenian hamster IgG,

BioXCell) on day 7 of DOCA-salt. Delivery of losartan (5 μg h^{-1}) or saline i.c.v. was started on the same day as DOCA-pellet implantation.

Isolation of brain and dural leukocytes

Isolation of brain leukocytes was performed as described[31]. Mice were anesthetized with pentobarbital (100 mg kg^{-1}, i.p.) and transcardially perfused with heparinized PBS. Brain cell isolation was performed by enzymatic digestion with Liberase DH (Roche Diagnostics) and Dispase (Worthington). Brain hemispheres were separated from the cerebellum and olfactory bulb and gently triturated in Hepes–HBSS buffer containing the following: 138 mM NaCl, 5 mM KCl, 0.4 mM Na_2HPO_4, 0.4 mM KH_2PO_4, 5 mM d-glucose and 10 mM Hepes using a Gentle MACS dissociator (Miltenyi Biotec) following the manufacturer's instructions. The dura was stripped from the skull[82] using a dissection microscope. The suspension was digested with 125 μg ml^{-1} of Liberase, 0.8 U ml^{-1} of dispase and 50 U ml^{-1} of DNase I at 37 °C for 45 min (brain) or 15 min (dura) in an orbital shaker at 100 r.p.m. Brain cells isolated were washed and subjected to 30% Percoll (GE Healthcare) density gradient centrifugation at 500*g* for 15 min. Dura were placed on the surface of a premoistened 70-μm cell strainer. Tissue was gently homogenized with the end of a 1-ml syringe plunger, washed with 20 ml of 2% FBS in PBS and centrifuged at 500*g* for 7 min.

ROS assessment by flow cytometry

After isolation of brain leukocytes, cells were incubated with dihydroethidium (DHE, 2.5 μM) or dichlorodihydrofluorescein diacetate (DCF; 2 μM) in stimulation buffer (RPMI-1640, 10% (v:v) heat-inactivated FBS, 100 units ml^{-1} of penicillin and 100 μg ml^{-1} of streptomycin) for 30 min at 37 °C and 5% CO_2. Some cells were pooled and separated for stimulation experiments, and incubated with PBS, murine recombinant IL-17 (10 ng ml^{-1}, Preprotech) or Ang II (300 nM, Sigma-Aldrich) for 30 min before addition of DHE (as above). Cells were washed with FACS buffer (1× PBS, 2% FBS and 0.05% NaN_3) and centrifuged at 500*g* for 7 min.

BM transplantation

As previously described[21,31], whole-body irradiation was performed on 6-week-old C57BL/6 male mice with a lethal dose of 9.5 Gy of γ-radiation using a ^{137}Cs source (Nordion Gammacell 40 Exactor). After 18 h, BM cells (2×10^6, i.v.) isolated from donor IL-17RA KO mice or B6.129S-*Cybb*^{tm1Din}/J mice (*Nox2*$^{-/-}$, JAX stock no. 002365) were transplanted in irradiated mice. Mice with transplanted BM cells were housed in cages with a Sulfatrim diet for the first 2 weeks.

RT–qPCR

Procedures for RT–qPCR were identical to those previously described[21,22,31]. Briefly, samples were collected in TRIzol (Invitrogen Life Technologies) and RNA was extracted according to the manufacturer's instructions. RNA samples were treated with RNase-free DNase I (Roche) to remove DNA contamination. Complementary DNA was produced from mRNA samples using the iScript Reverse Transcription Supermix (BioRad). Quantitative determination of gene expression was performed on a Quantstudio 5 (Applied Biosystems).

Hypoxanthine–guanine phosphoribosyltransferase was used to normalize gene expression. RT–qPCR was conducted with cDNA in duplicate 10-µl reactions on a 384-well plate using the Maxim SYBR Green/ROX qPCR Master Mix (2×) (Thermo Fisher Scientific). The reactions were incubated at 50 °C for 2 min and then at 95 °C for 10 min. A PCR-cycling protocol consisting of 15 s at 95 °C and 1 min at 60 °C for 45 cycles was used for quantification. Relative expression levels were calculated according to Livak and Schmittgen and values were normalized to respective normal control samples. Reference primer sequences are described in Supplementary Table 4.

For assessment of *Il17ra* knockdown in vivo, genomic DNA was extracted from sorted endothelial and microglia cells. Cre recombination specifically targets exons 4–7 of the *Il17ra* gene in IL-17RA$^{flox/flox}$ mice, thus we normalized *Il17ra* exon 5 expression to the nontargeted *Il17ra* exon 3. Primer sequences are described in Supplementary Table 4.

RNAscope

Tissue was treated according to manufacture's instructions for the RNAscope Multiplex Fluorescent v.2 Assay. After 2% PFA perfusion, brain tissue was left in 2% PFA overnight. The tissue then went through a sequential sucrose gradient (10%, 20%, 30%) before freezing and storing at −80 °C. Tissue was cut at 10 µm on a cryostat, mounted on charged slides and stored at −80 °C until use. Slides were left to warm up for 2 h at −20 °C, then baked at 60 °C for 30+ min. Slides were washed with 1× PBS for 5 min, then treated with RNAscope hydrogen peroxide for 10 min. Slides were washed with nuclease-free water and pretreated with target retrieval buffer in a slide envelope placed in 100 °C boiling water for 5 min. Slides were then washed with distilled water, dipped in 100% EtOH and a barrier was established around the tissue using a hydrophobic marker. Slides were then allowed to air dry overnight. Slides were treated with protease IV for 15 min at 40 °C, followed by a probe incubation for 2 h at 40 °C. The probes (purchased from ACD) used were Mm-Mrc1 (catalog no. 437511) and Mm-Il17ra-O1-C2 (catalog no. 566131-C2). A three-plex positive control probe and three-plex negative control were run concurrently. After probe incubation, slides underwent three amplification steps (RNAscope Multiplex Fluorescent Detection Reagents v.2, ACD, catalog no. 323110) followed by the development of HRP signal fluorescence with tyramide signal amplification-based fluorophores. HRP blockers were used after every fluorophore incubation. After each step, slides were washed twice with wash buffer. Slides were treated with RNAscope DAPI for 30 s then cover-slipped in Fluorosave Reagent (Sigma-Aldrich, catalog no. 345789) and left to dry for 20 min. Slides were then stored at 4 °C until imaging.

IL-17A ELISpot assay

Dura leukocytes were isolated as described above and incubated on an ELISpot plate for 4 h in stimulation buffer (RPMI-1640, 10% (v:v) heat-inactivated FBS, 100 units ml^{-1} of penicillin, 100 µg ml^{-1} of streptomycin, 100 ng ml^{-1} of phorbol 12-myristate 13-acetate and 1 µg ml^{-1} of ionomycin) in a 37 °C humidified incubator with 5% CO_2. Mouse IL-17A ELISpotPLUS kit ALP (MABTECH, catalog no. 3521-4APW-2) was performed following the manufacturer's instructions. Wells were developed with 5-bromo-4-chloro-3-indolyl-1-phosphate and nitroblue tetrazolium-plus for 15 min and color development was stopped by

washing with diH_2O. Images were obtained using a digital camera (T TAKMLY, MX200-B) and analyzed using ImageJ software.

CSF collection

Mice were anesthetized with isoflurane (3% induction, 1.5% maintenance) and placed on a stereotaxic frame with the head slightly tilted forward. A small incision was made over the back of the neck and muscle tissue moved to expose the dura over the cisterna magna. The area was cleaned with a cotton bud. Heparinized glass capillaries were prepared using a micropipette puller, attached to a thin tube and syringe connected through a three-way valve and mounted on a micromanipulator[88]. Under a dissecting microscope, the glass capillary was aligned to the cisterna magna, avoiding blood vessels in the area, and tapped through the dura to collect CSF for a maximum of 10 min. On average, 15–18 μl was obtained per mouse. Equal volumes of CSF from two animals were pooled to maximize a loading sample volume of 25 μl for IL-17 quantification (Mesoscale).

Ang II assay

Mice were euthanized and blood was collected by cardiac puncture in a prechilled tube containing a mix of protease inhibitors. Plasma was collected and transferred to a prechilled tube and stored frozen at −80 °C. Brains were collected and immediately frozen on dry ice. Ang II concentration was determined using a radioimmunoassay by the Hypertension Core Laboratory of the Wake Forest University School of Medicine (Winston-Salem, NC, USA)[89].

Statistics and reproducibility

Sample size was determined according to standard power analysis (80% power and $\alpha = 0.05$) based on Cohen's d standardized effect sizes calculated from published studies[21,22,28,80,90]. The sample sizes in the present study are similar to those reported in these previous publications. Animals were randomly assigned to treatment and control groups. Whenever feasible, data collection was performed by a blinded experimenter. Data analysis was performed in a blinded fashion. After testing for normality (Shapiro–Wilk test), intergroup differences were analyzed by unpaired, two-tailed Student's t-test for single comparison, or by one-way or two-way analysis of variance (ANOVA) with Tukey's or Bonferroni's multiple-comparison test, as appropriate, and indicated in the figure legends. If nonparametric testing was indicated, intergroup differences were analyzed by Mann–Whitney U-test or Kruskal–Wallis test with Dunn's correction, as appropriate, and indicated in the figure legends. The F test for equality of variances was performed and, if indicated, appropriate corrections were made (Welch's correction for the t-test). Statistical tests through the manuscript were performed using Prism 9 (GraphPad). All data are presented as mean ± s.e.m. For rigor and reproducibility, experiments were repeated at least three times throughout the manuscript.

Extended Data

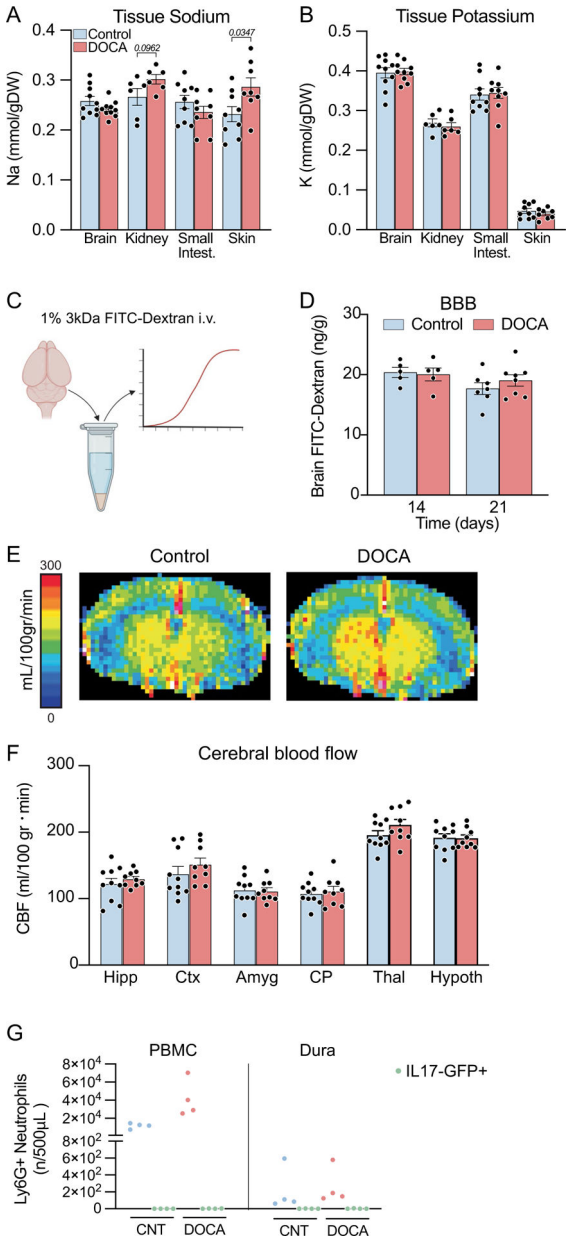

Extended Data Fig. 1 |. Physiological parameters at 21 days of DOCA-salt HTN.

(A-B) Tissue sodium (**A**) and potassium (**B**) content was assessed by inductively coupled plasma – atomic emission spectrometry (ICP-AES)[75,76]. Intergroup differences analyzed by unpaired two-tailed t-test for each organ, n = 6–10 mice/group as shown. **(C-D)** BBB permeability (**D**) assessed by brain extravasation of 3 kDa FITC-dextran (**C**) quantified by spectrophotometry in brain homogenates revealed no impairment during DOCA-salt hypertension (n = 5–8). **(E-F)** DOCA-salt HTN does not impair resting CBF assessed quantitatively by arterial spin label (ASL)-MRI (control (**E**) n = 10 mice, DOCA (**F**) n = 9 mice) at 21 days of treatment in the hippocampus (Hipp), cortex (Ctx), amygdala (Amyg), caudate putamen (CP), thalamus (Thal), or hypothalamus (Hypoth). Intergroup differences

analyzed by two-way ANOVA with Tukey's multiple comparisons test. **(G)** IL17-GFP+ neutrophils were not changed by DOCA-salt in peripheral blood mononuclear cells (PBMC) or in the dura. n = 4/group.

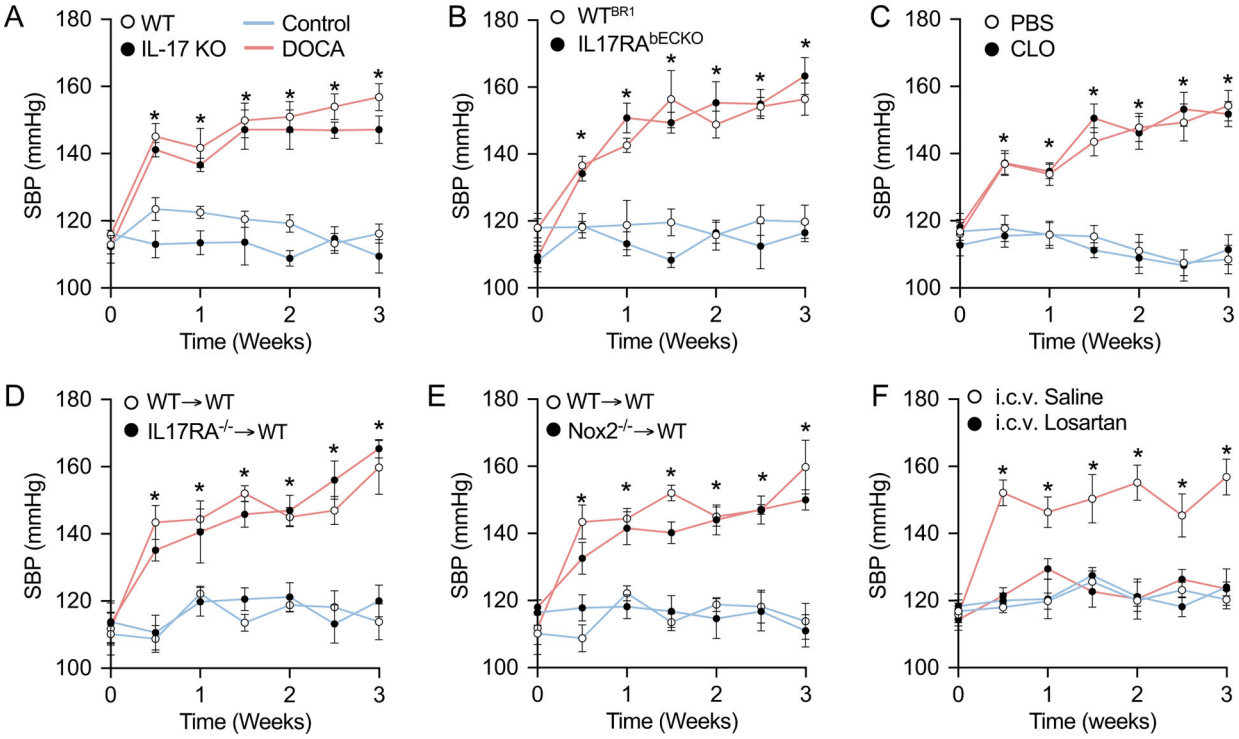

Extended Data Fig. 2 |. Systolic blood pressure measured by tail-cuff plethysmography.
Systolic blood pressure (SBP) was assessed twice per week in all control and DOCA-salt mice of the following groups: **(A)** wild-type (WT, n = 10 mice) and IL17-deficient (IL17KO, n = 6 mice) mice, **(B)** WT^{BR1} (n = 5 mice/group) and IL17RA brain endothelial cell knockout ($IL17RA^{bECKO}$, n = 6 mice/group), **(C)** mice treated with vehicle (PBS) or clodronate (CLO)-containing liposomes (n = 10 mice/group), **(D** and **E)** bone marrow chimeras (n = 5 mice/group), and **(F)** i.c.v. saline or losartan (n = 6 mice/group). Intergroup differences analyzed by two-way repeated measures ANOVA with Tukey's multiple comparisons test.

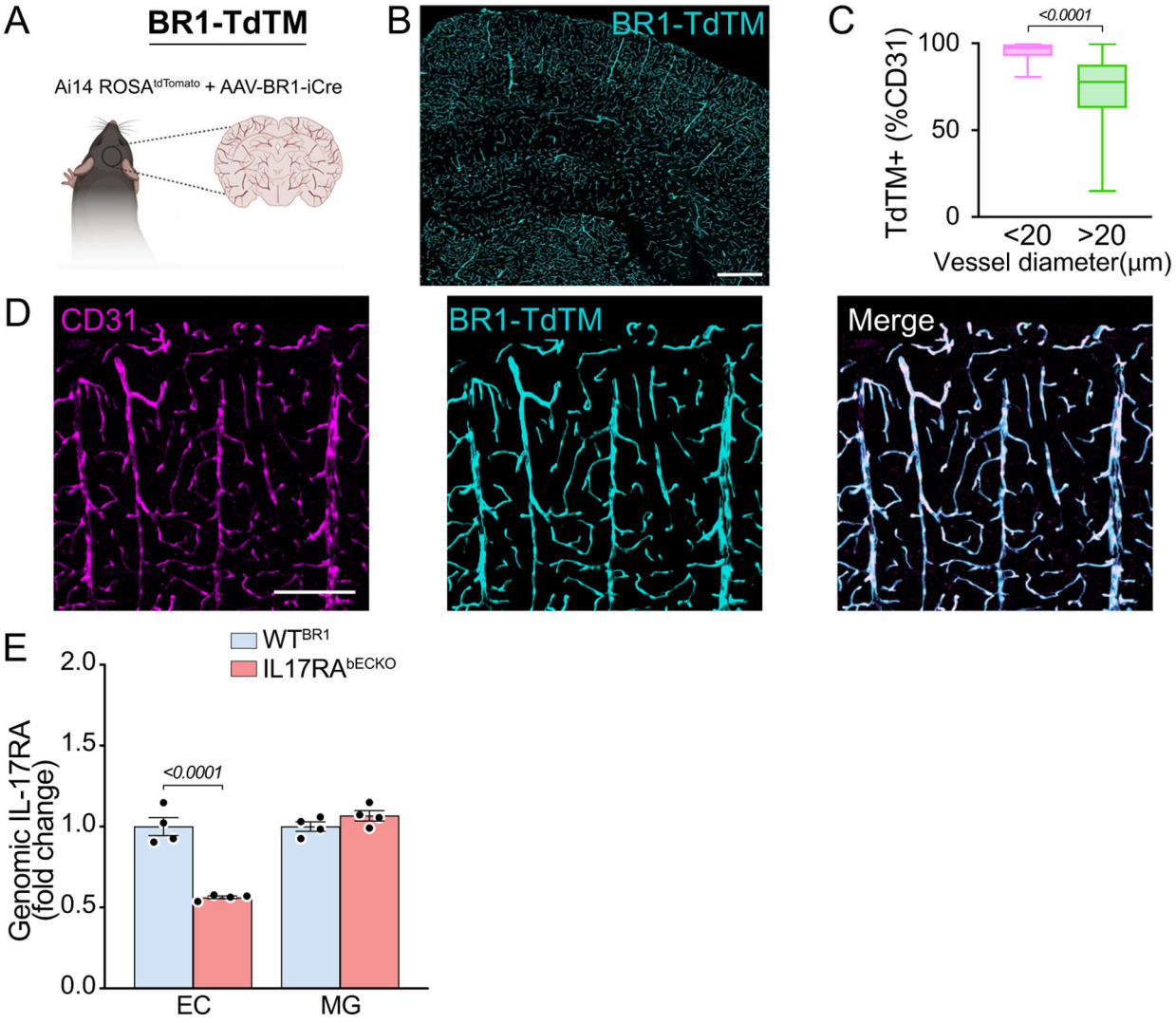

Extended Data Fig. 3 |. Cerebral endothelial cell specific Cre delivery with AAV-BR1-iCre.
(A) AAV-BR1-iCre delivery in Ai14-ROSA^{tdTomato} reporter mice demonstrates **(B)** widespread TdTomato (TdTM) expression in cerebral vessels. Scale bar: 500μm. **(C)** Specifically, we observed a 90–95% endothelial viral transduction in vessels less than 20μm (n = 5 mice, 110 vessels per mouse). **(D)** Representative images of TdTM expression in CD31+ endothelial cells. Scale bar: 150μm. **(E)** Quantification of genomic IL-17RA deletion in EC and MG (n = 4 mice/group). Intergroup differences analyzed by two-way ANOVA with Tukey's multiple-comparison test.

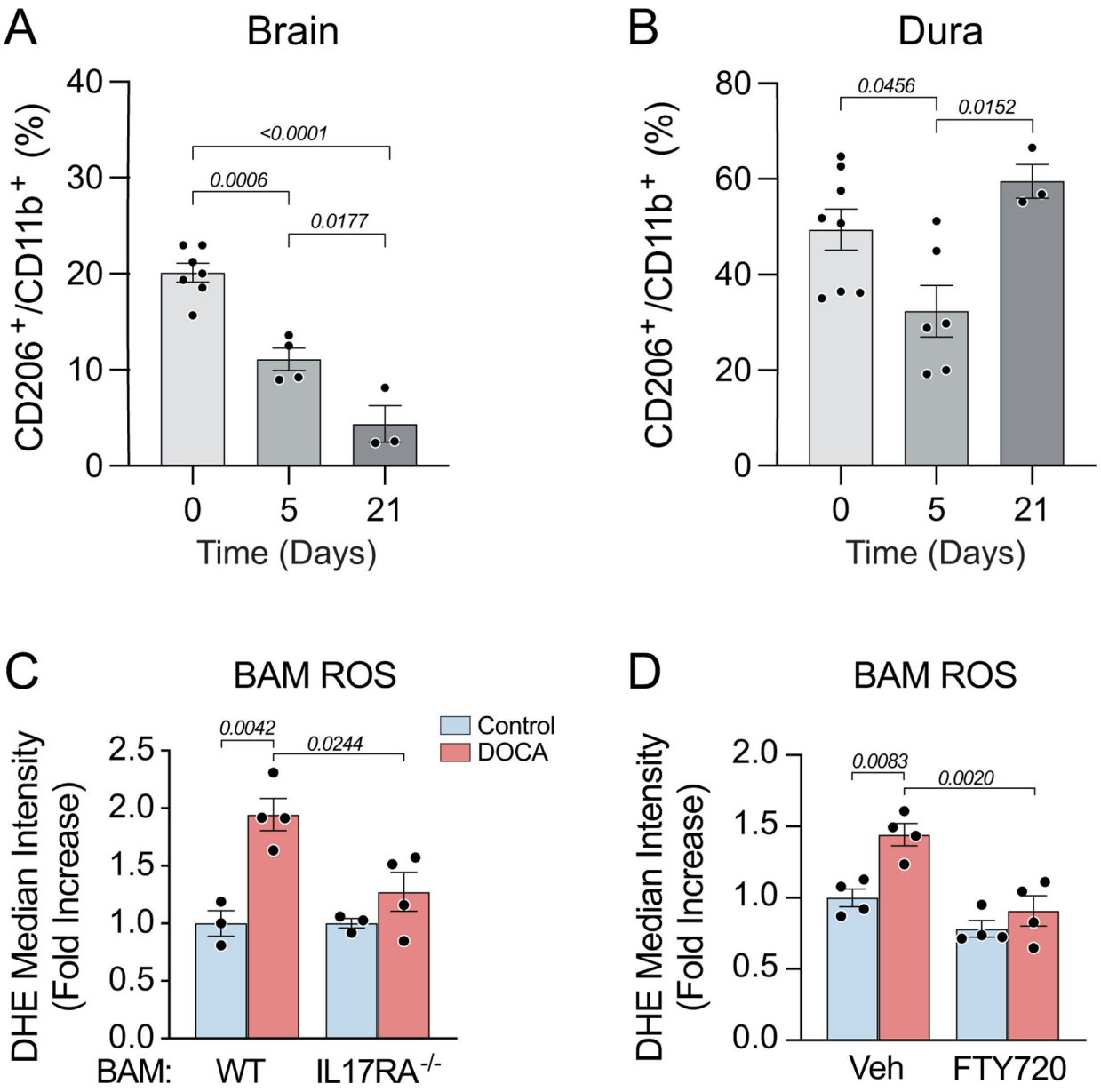

Extended Data Fig. 4 |. Brain macrophages depletion with clodronate and ROS measurement. **(A)** i.c.v. clodronate depletes brain macrophages for 21 days, and **(B)** initially depletes dura macrophages, but they are fully restored within 21 days. n = 3–7 mice/group as shown. Intergroup differences analyzed by one-way ANOVA with Tukey's multiple-comparison test. **(C)** DOCA-salt does not increase BAM ROS IL17RA$^{-/-}$→WT chimeras (control n = 3 mice, DOCA n = 4 mice), or **(D)** in WT mice treated with FTY720 (n = 4 mice/group). Intergroup differences analyzed by two-way ANOVA with Tukey's multiple comparisons test.

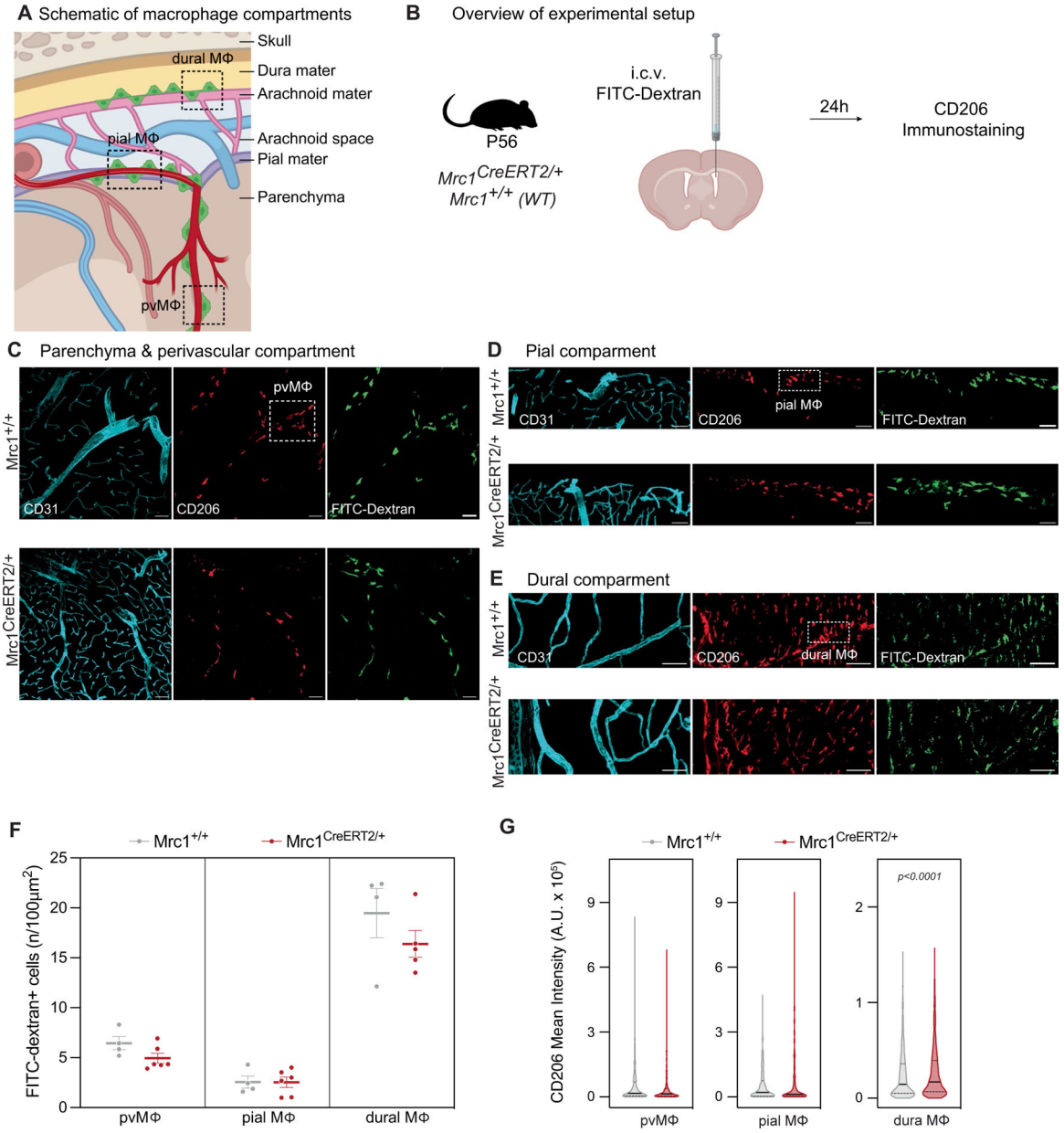

Extended Data Fig. 5 |. Novel Mrc1$^{CreERT2/+}$ mouse.

(A) Schematic of CNS macrophage compartments. **(B)** Illustration of the experimental procedure for intracerebroventricular (i.c.v.) FITC-Dextran injection and analysis of adult Mrc1$^{+/+}$ or Mrc1$^{CreERT2/+}$. **(C-E)** Immunofluorescence images reveals FITC-Dextran (green) (**c**) in BAMs (CD206 + , red) in perivascular macrophages (pvMΦ) and pial MΦ (**D**) and dural MΦ (**E**) compartments in the cortex of adult Mrc1$^{+/+}$ or Mrc1$^{CreERT2/+}$ mice. CD31+ blood vessels shown in cyan. Scale bars: 20 µm. **(F)** Quantification of pvMΦ, pial MΦ and dural MΦ in *Mrc1$^{+/+}$* (n = 4 mice) or *Mrc1$^{CreERT2/+}$* (n = 6 mice for of pvMΦ and pial MΦ, n = 5 mice for dural MΦ). Data shown as mean ± SEM; intergroup differences analyzed by two-way ANOVA with Bonferroni's multiple comparison test. **(G)** CD206 surface expression levels on individual FITC-Dextran cells (pvMΦ *Mrc1$^{+/+}$* n = 586 cells,

Mrc1$^{CreERT2/+}$ n = 676 cells; pial *Mrc1*$^{+/+}$ n = 235 cells, *Mrc1*$^{CreERT2/+}$ n = 340 cells; dural *Mrc1*$^{+/+}$ n = 1780 cells, *Mrc1*$^{CreERT2/+}$ n = 1871 cells. *Mrc1*$^{+/+}$ n = 4 mice, *Mrc1*$^{CreERT2/+}$ n = 6 mice for of pvMΦ and pial MΦ, n = 5 mice for dural MΦ; 10 images per mouse per compartment, all cells within each image were analyzed). Intergroup differences analyzed by unpaired two-tailed Mann Whitney test; lines in violin plot indicate median and quartiles.

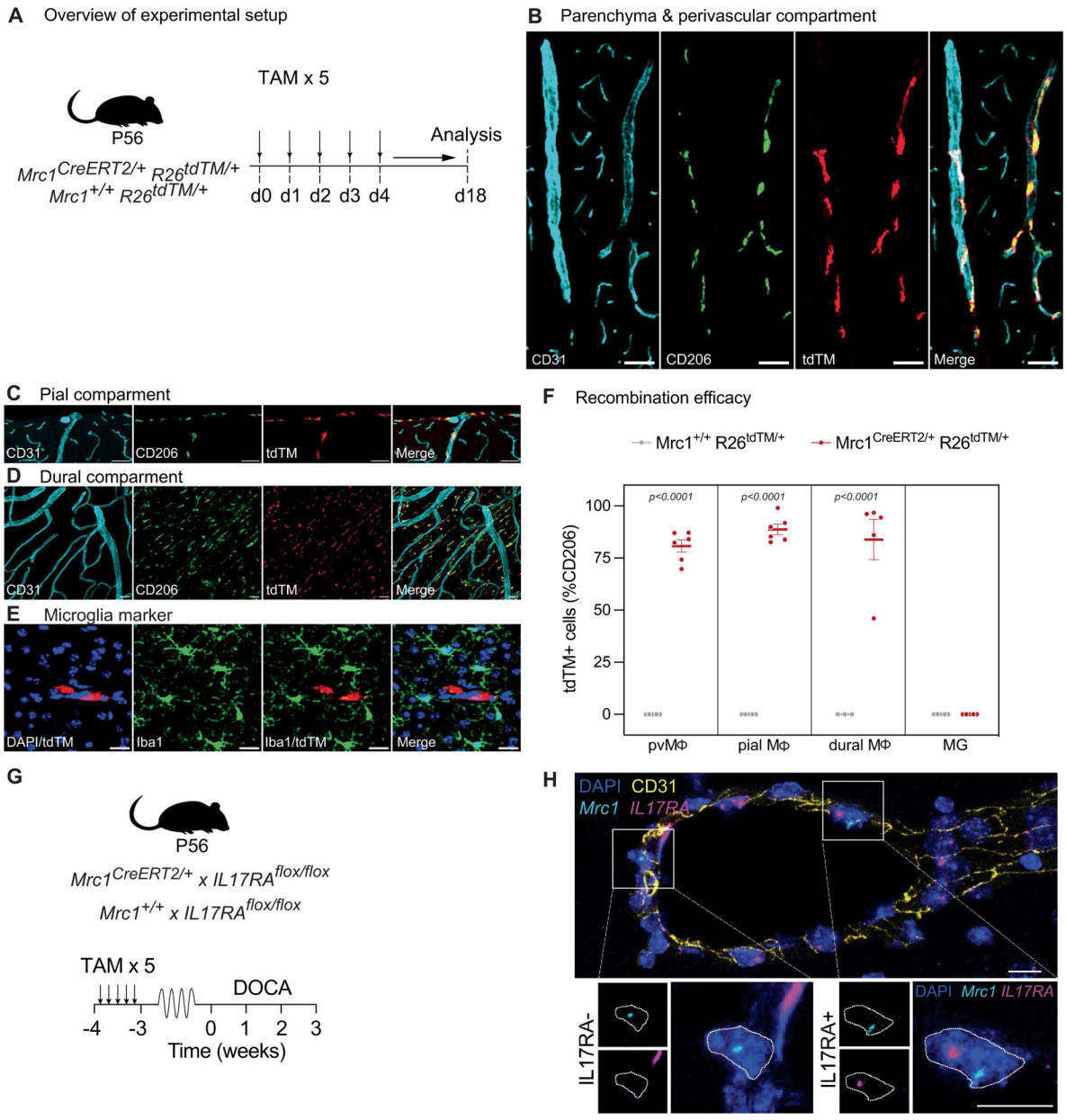

Extended Data Fig. 6 |. Novel Mrc1$^{CreERT2/+}$ mouse.

(A) Experimental procedure for tamoxifen administration (TAM) and analysis of adult *Mrc1*$^{+/+}$*R26*$^{tdTM/+}$ or *Mrc1*$^{CreERT2/+}$*R26*$^{tdTM/+}$ mice. **(B-D)** Immunofluorescence images reveal tdTM^{+} (red) in CD206^{+} BAM (green) in perivascular macrophages (pvMΦ) (**B**), pial MΦ (**c**), and dural MΦ (**D**). CD31^{+} blood vessels shown in cyan. Scale bars: 20 μm**. (E)**

TdTM expression was no observed in microglia (IBA1$^+$, green) of adult *Mrc1*$^{CreERT2/+}$*R26*$^{tdTM/+}$ mice. Scale bars: 20 μm**. (F)** Quantification of recombination efficacy in pvMΦ, pial MΦ, and dural MΦ, as well as microglia in *Mrc1*$^{+/+}$*R26*$^{tdTM/+}$ and *Mrc1* $^{CreERT2/+}$*R26*$^{tdTM/+}$ mice. Data shown as mean ± SEM; *Mrc1*$^{+/+}$*R26*$^{tdTM/+}$ n = 5 mice per compartment except n = 3 mice for dura; and *Mrc1*$^{CreERT2/+}$*R26*$^{tdTM/+}$ n = 6 mice for pvMΦ and pial, and n = 5 mice for dural and microglia. **(G)** Experimental procedure for tamoxifen administration and analysis of Mrc1$^{CreERT2/+}$ x IL17RA$^{flox/flox}$ mice. **(H)** Representative image of cerebral blood vessel stained for CD31 (yellow, IHC), Mrc1 (cyan, RNAscope) and IL17RA (magenta, RNAscope). Blood vessel shows one IL17RA- BAM and one IL17RA + BAM. This identification strategy was used for quantification of IL17RA deletion in Mrc1$^{CreERT2/+}$ x IL17RA$^{flox/flox}$ mice. Scale bars: 10 μm.

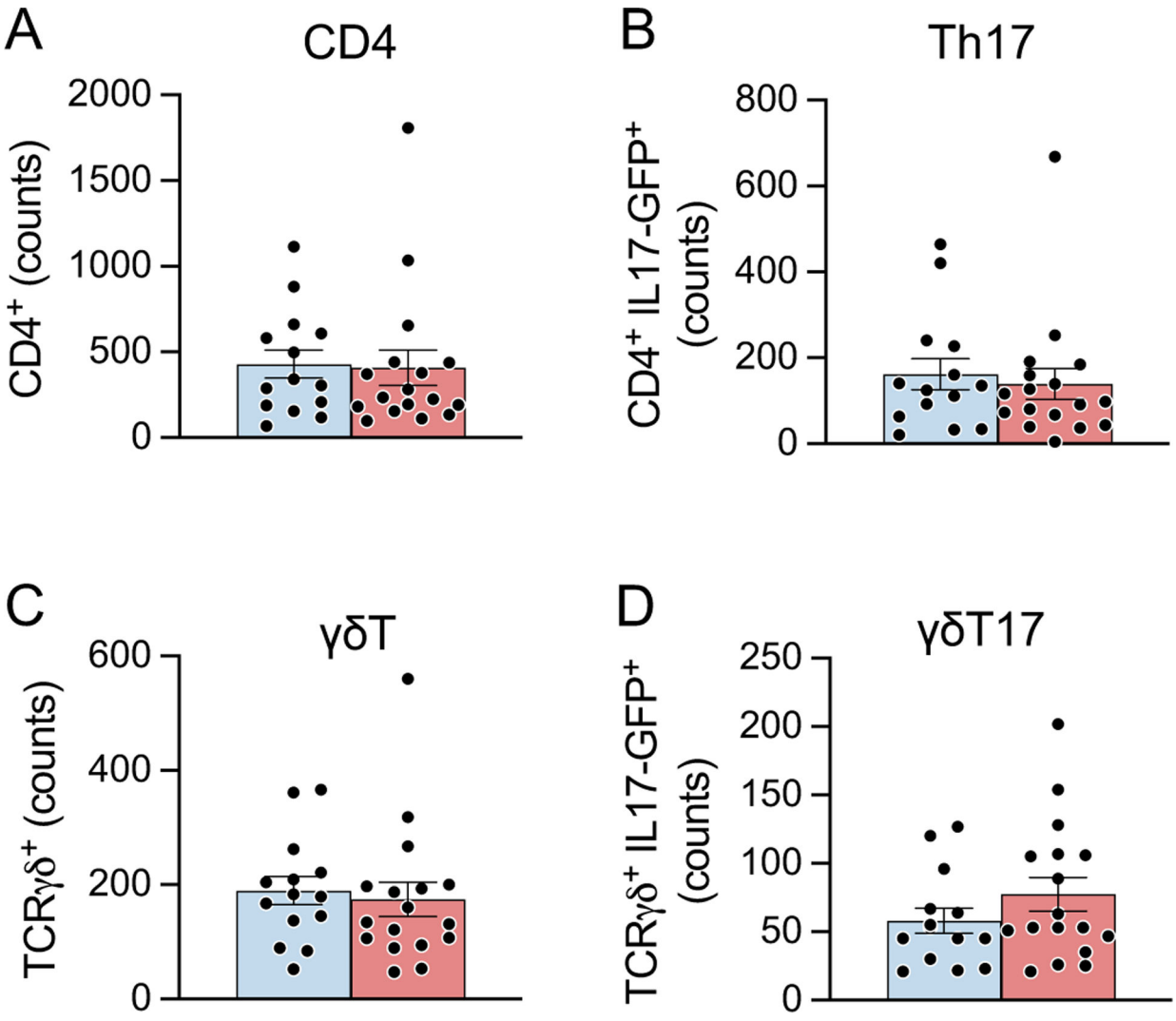

Extended Data Fig. 7 |. Total numbers of cells obtained by flow cytometry in dura.
Total numbers of cells obtained by flow cytometry from control (n = 14 mice) and DOCA (n = 17 mice) dura samples. **(A)** Total CD4 cells. **(B)** Total Th17 cells. **(C)** Total γδT cells. **(D)**Total γδT17 cells.

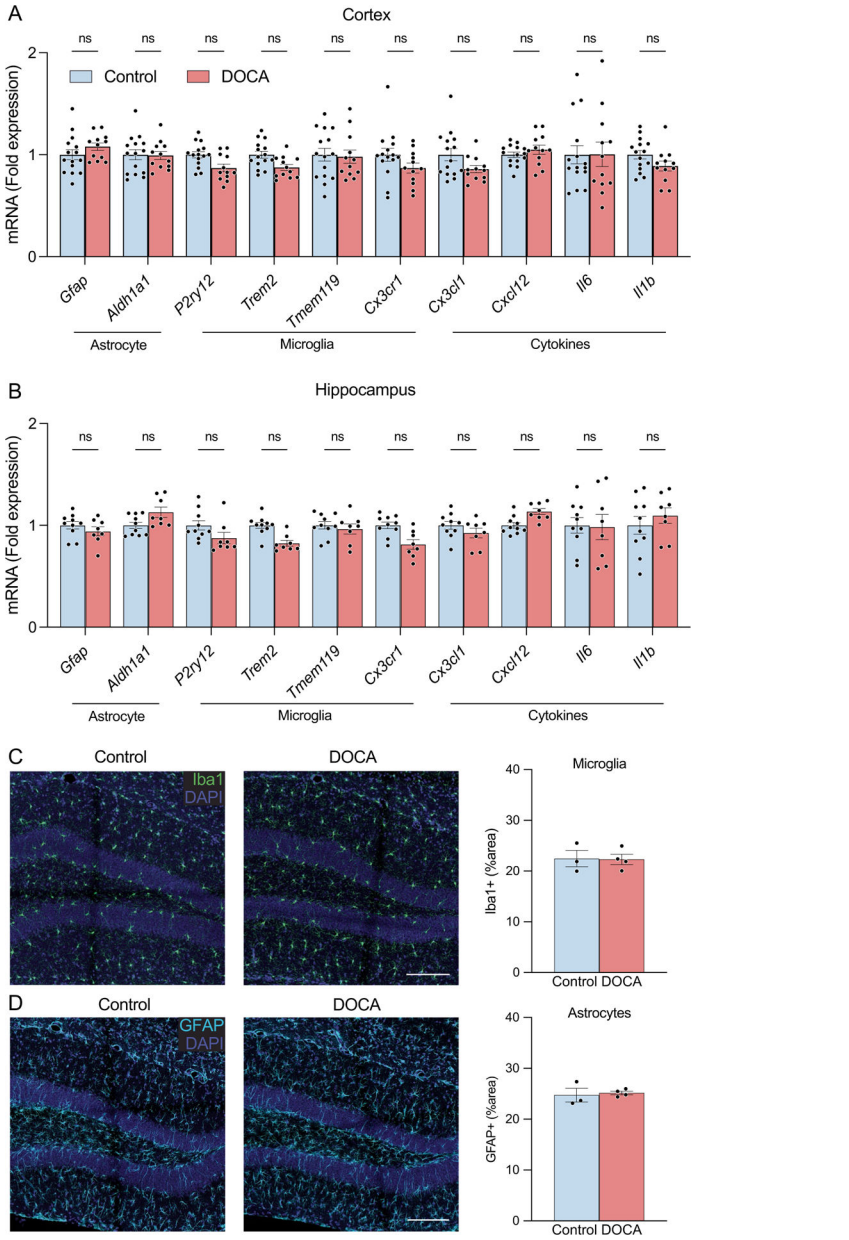

Extended Data Fig. 8 |. Markers of neuroinflammation in neocortex and hippocampus.
(A-B) Selected inflammatory gene expression assessed by qPCR was not altered in cortex (**A**) (control n = 15 mice; DOCA n = 12 mice) or hippocampus (**B**) of DOCA-salt mice (control n = 10 mice; DOCA n = 8 mice). Intergroup differences analyzed by two-way ANOVA with Tukey's multiple comparison test. **(C)** Iba1+ microglia and **(D)** GFAP+ astrocyte area was not altered in the hippocampus of DOCA-salt (control n = 3 mice, DOCA n = 4 mice). Intergroup differences analyzed by unpaired two-tailed t-test. Scale bars: 150 μm.

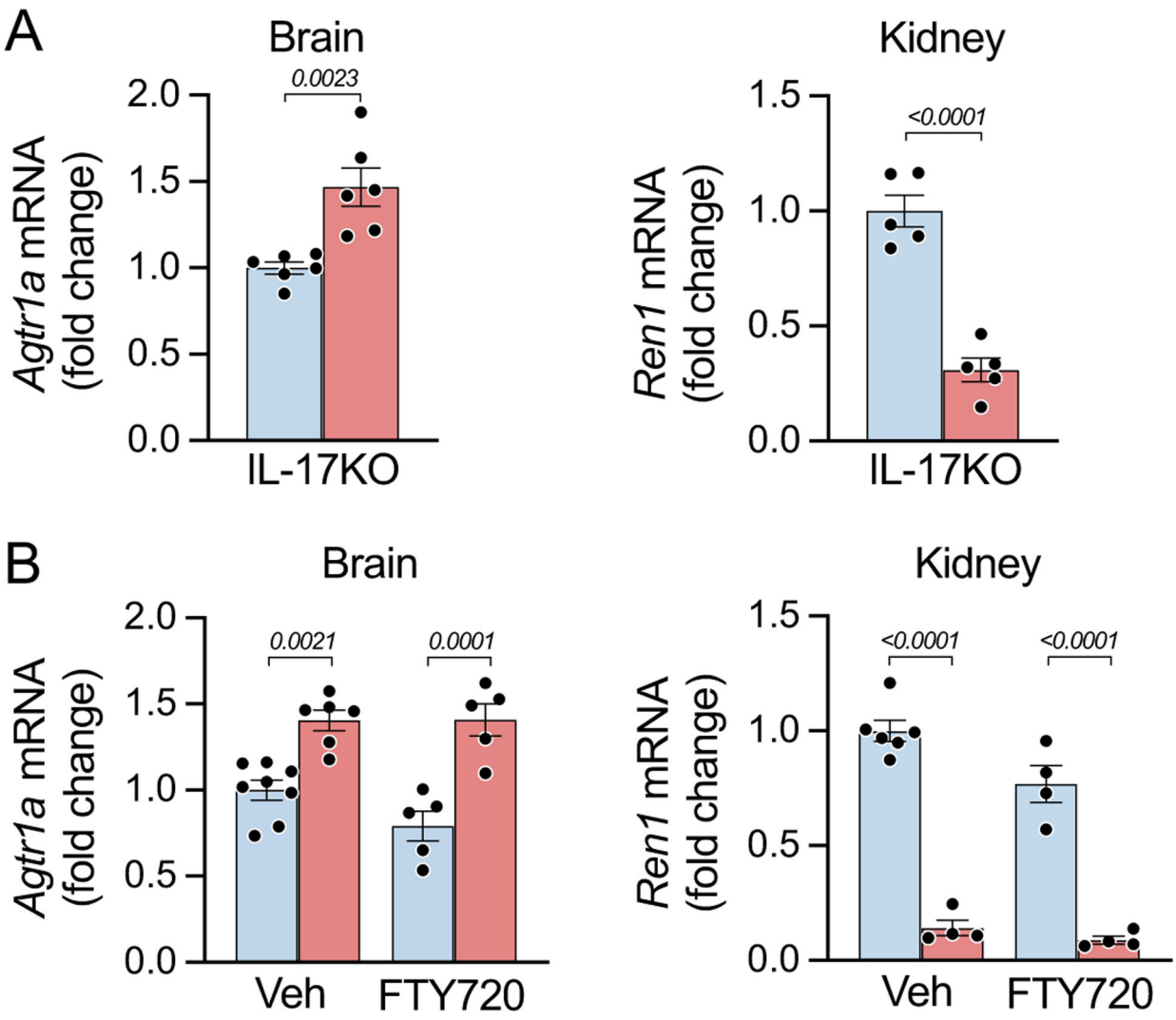

Extended Data Fig. 9 |. Brain *Agtr1a* and renal *Ren1* mRNA expression.

Brain *Agtr1a* and renal *Ren1* mRNA expression in **(A)** IL-17KO (brain n = 6 mice/group, kidney n = 5 mice/group) and **(B)** vehicle and FTY720-treated control and DOCA-salt mice (n = 4–8 mice/group as shown). Intergroup differences analyzed by unpaired two-tailed t-test (A) or two-way ANOVA with Tukey's multiple comparison test (B).

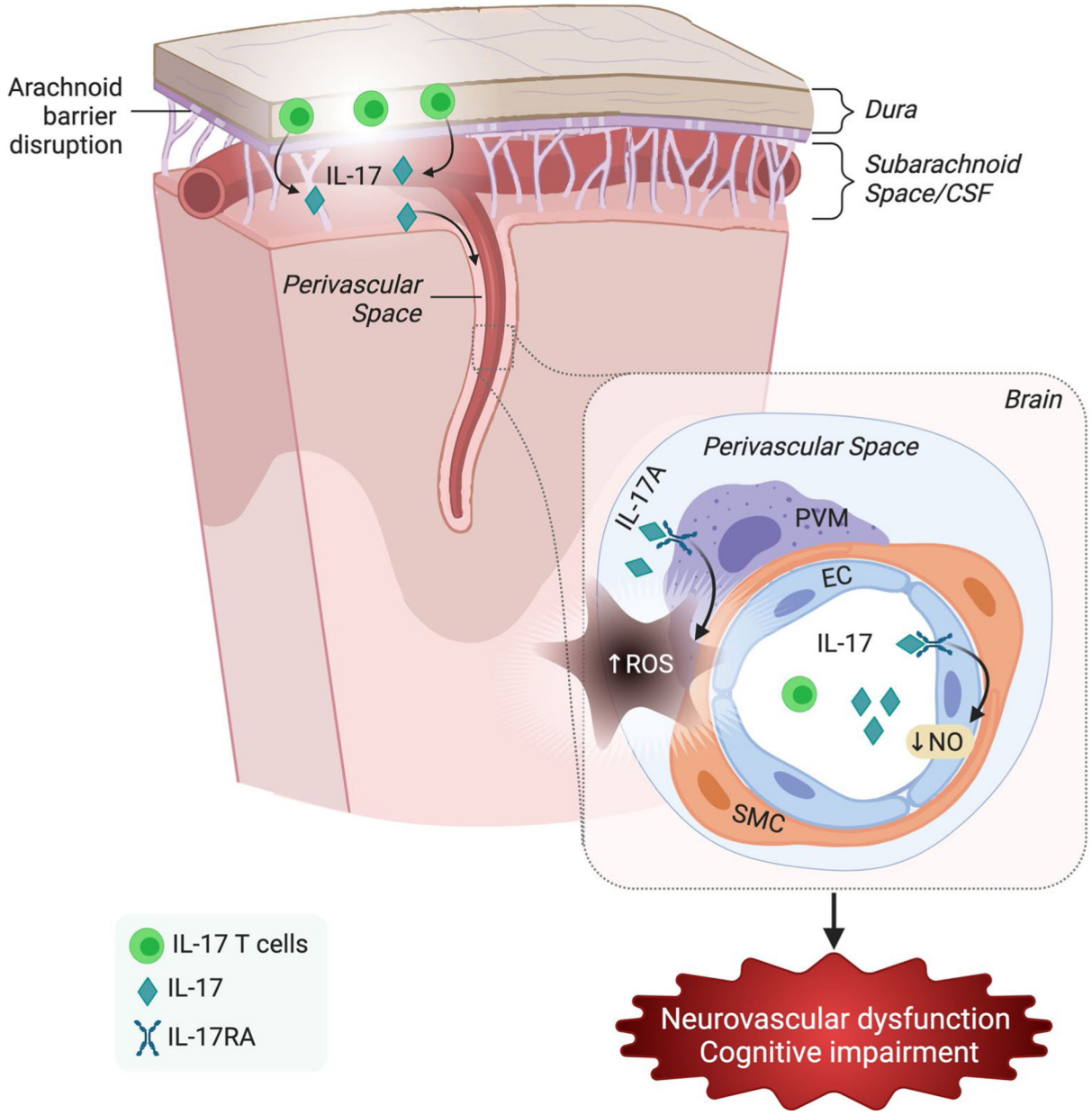

Extended Data Fig. 10 |. Summary diagram.

Summary of the mechanisms by which DOCA-salt hypertension alters neurovascular and cognitive function in mice. These effects are mediated by concurring actions of IL17 acting on IL17RA on different cells types on both sides of the BBB. In the circulation, IL-17 produced by T-cells acts on cerebral endothelial IL-17RA to reduce NO production leading to suppression of endothelial vasoactivity without affecting the increase in CBF induced by neural activity. In the brain, IL-17 produced by dura T-cells acts on IL-17RA on BAM to induce vascular oxidative stress and suppression of functional hyperemia with minimal effects on endothelial function.

Supplementary Material

Refer to Web version on PubMed Central for supplementary material.

Acknowledgements

This work was supported by grants from the National Institutes of Health (nos. R37-NS089323 and R01-NS095441 to C.I. and K22-NS123507 to M.M.S.), as well as the Leon Levy Fellowship in Neuroscience (to M.M.S.). The support from the Feil Family Foundation is gratefully acknowledged. Figure schematics were created with BioRender.com.

Data availability

Source data are provided with this paper. Any additional data requests are available from the corresponding authors upon request.

References

1. Levine DA, Springer MV & Brodtmann A Blood pressure and vascular cognitive impairment. Stroke 53, 1104–1113 (2022). [PubMed: 35264009]
2. Muntner P et al. Blood pressure control among us adults, 2009 to 2012 through 2017 to 2020. Hypertension 79, 1971–1980 (2022). [PubMed: 35616029]
3. Carey RM, Sakhuja S, Calhoun DA, Whelton PK & Muntner P Prevalence of apparent treatment-resistant hypertension in the United States. Hypertension 73, 424–431 (2019). [PubMed: 30580690]
4. Williamson JD et al. Effect of intensive vs standard blood pressure control on probable dementia: a randomized clinical trial. JAMA 321, 553–561 (2019). [PubMed: 30688979]
5. Webb AJS & Werring DJ New insights into cerebrovascular pathophysiology and hypertension. Stroke 53, 1054–1064 (2022). [PubMed: 35255709]
6. Iadecola C & Gottesman RF Neurovascular and cognitive dysfunction in hypertension: epidemiology, pathobiology and treatment. Circ. Res 124, 1025–1044 (2019). [PubMed: 30920929]
7. Oh YS et al. National Heart, Lung, and Blood Institute Working Group report on salt in human health and sickness: building on the current scientific evidence. Hypertension 68, 281–288 (2016). [PubMed: 27324228]
8. Elijovich F et al. Salt sensitivity of blood pressure: a scientific statement from the American Heart Association. Hypertension 68, e7–e46 (2016). [PubMed: 27443572]
9. Grobe JL et al. Angiotensinergic signaling in the brain mediates metabolic effects of deoxycorticosterone (DOCA)-salt in C57 mice. Hypertension 57, 600–607 (2011). [PubMed: 21263123]
10. Basting T & Lazartigues E DOCA-salt hypertension: an update. Curr. Hypertens. Rep 19, 32 (2017). [PubMed: 28353076]
11. Meade TW, Imeson JD, Gordon D & Peart WS The epidemiology of plasma renin. Clin. Sci 64, 273–280 (1983).
12. Alderman MH et al. Association of the renin-sodium profile with the risk of myocardial infarction in patients with hypertension. N. Engl. J. Med 324, 1098–1104 (1991). [PubMed: 1759997]
13. Madhur MS et al. Interleukin 17 promotes angiotensin II-induced hypertension and vascular dysfunction. Hypertension 55, 500–507 (2010). [PubMed: 20038749]
14. Yao W, Sun Y, Wang X & Niu K Elevated serum level of interleukin 17 in a population with prehypertension. J. Clin. Hypertens 17, 770–774 (2015).
15. Simundic T et al. Interleukin 17a and toll-like receptor 4 in patients with arterial hypertension. Kidney Blood Press. Res 42, 99–108 (2017). [PubMed: 28359064]
16. Kleinewietfeld M et al. Sodium chloride drives autoimmune disease by the induction of pathogenic Th17 cells. Nature 496, 518–522 (2013). [PubMed: 23467095]

17. Wu C et al. Induction of pathogenic Th17 cells by inducible salt-sensing kinase SGK1. Nature 496, 513–517 (2013). [PubMed: 23467085]
18. Kierdorf K, Masuda T, Jordao MJC & Prinz M Macrophages at CNS interfaces: ontogeny and function in health and disease. Nat. Rev. Neurosci 20, 547–562 (2019). [PubMed: 31358892]
19. Faraco G et al. Hypertension enhances Aβ-induced neurovascular dysfunction, promotes β-secretase activity, and leads to amyloidogenic processing of APP. J. Cereb. Blood Flow. Metab 36, 241–252 (2016). [PubMed: 25920959]
20. Kopp C et al. ^{23}Na magnetic resonance imaging-determined tissue sodium in healthy subjects and hypertensive patients. Hypertension 61, 635–640 (2013). [PubMed: 23339169]
21. Faraco G et al. Perivascular macrophages mediate the neurovascular and cognitive dysfunction associated with hypertension. J. Clin. Invest 126, 4674–4689 (2016). [PubMed: 27841763]
22. Faraco G et al. Dietary salt promotes neurovascular and cognitive dysfunction through a gut-initiated Th17 response. Nat. Neurosci 21, 240–249 (2018). [PubMed: 29335605]
23. Toda N, Ayajiki K & Okamura T Cerebral blood flow regulation by nitric oxide: recent advances. Pharm. Rev 61, 62–97 (2009). [PubMed: 19293146]
24. Iadecola C et al. The neurovasculome: key roles in brain health and cognitive impairment: a scientific statement from the American Heart Association/American Stroke Association. Stroke 54, e251–e271 (2023). [PubMed: 37009740]
25. Itani HA et al. Activation of human T cells in hypertension: studies of humanized mice and hypertensive humans. Hypertension 68, 123–132 (2016). [PubMed: 27217403]
26. Kim S et al. Imbalance of gut microbiome and intestinal epithelial barrier dysfunction in patients with high blood pressure. Clin. Sci 132, 701–718 (2018).
27. Esplugues E et al. Control of Th17 cells occurs in the small intestine. Nature 475, 514–518 (2011). [PubMed: 21765430]
28. Benakis C et al. Commensal microbiota affects ischemic stroke outcome by regulating intestinal gammadelta T cells. Nat. Med 22, 516–523 (2016). [PubMed: 27019327]
29. Maeda Y et al. Il-17-producing vγ4+ γδ T cells require sphingosine 1-phosphate receptor 1 for their egress from the lymph nodes under homeostatic and inflammatory conditions. J. Immunol 195, 1408–1416 (2015). [PubMed: 26170380]
30. Korbelin J et al. A brain microvasculature endothelial cell-specific viral vector with the potential to treat neurovascular and neurological diseases. EMBO Mol. Med 8, 609–625 (2016). [PubMed: 27137490]
31. Santisteban MM et al. Endothelium-macrophage crosstalk mediates blood-brain barrier dysfunction in hypertension. Hypertension 76, 795–807 (2020). [PubMed: 32654560]
32. El Malki K et al. An alternative pathway of imiquimod-induced psoriasis-like skin inflammation in the absence of interleukin-17 receptor a signaling. J. Invest Dermatol 133, 441–451 (2013). [PubMed: 22951726]
33. Schaeffer S & Iadecola C Revisiting the neurovascular unit. Nat. Neurosci 24, 1198–1209 (2021). [PubMed: 34354283]
34. Nikolakopoulou AM et al. Endothelial LPR1 protects against neurodegeneration by blocking cyclophilin A. J. Exp. Med 218, e20202207 (2021). [PubMed: 33533918]
35. Van Hove H et al. A single-cell atlas of mouse brain macrophages reveals unique transcriptional identities shaped by ontogeny and tissue environment. Nat. Neurosci 22, 1021–1035 (2019). [PubMed: 31061494]
36. Park L et al. Brain perivascular macrophages initiate the neurovascular dysfunction of Alzheimer abeta peptides. Circ. Res 121, 258–269 (2017). [PubMed: 28515043]
37. Sayd A et al. Depletion of brain perivascular macrophages regulates acute restraint stress-induced neuroinflammation and oxidative/nitrosative stress in rat frontal cortex. Eur. Neuropsychopharmacol 34, 50–64 (2020). [PubMed: 32245674]
38. Mendiola AS et al. Transcriptional profiling and therapeutic targeting of oxidative stress in neuroinflammation. Nat. Immunol 21, 513–524 (2020). [PubMed: 32284594]

39. Ivan DC, Walthert S, Berve K, Steudler J & Locatelli G Dwellers and trespassers: mononuclear phagocytes at the borders of the central nervous system. Front Immunol. 11, 609921 (2020). [PubMed: 33746939]
40. Garcia-Bonilla L et al. Role of microglial and endothelial CD36 in post-ischemic inflammasome activation and interleukin-1β-induced endothelial activation. Brain Behav. Immun 95, 489–501 (2021). [PubMed: 33872708]
41. Hohsfield LA et al. Effects of long-term and brain-wide colonization of peripheral bone marrow-derived myeloid cells in the CNS. J. Neuroinflamm 17, 279 (2020).
42. Chinnery HR, Ruitenberg MJ & McMenamin PG Novel characterization of monocyte-derived cell populations in the meninges and choroid plexus and their rates of replenishment in bone marrow chimeric mice. J. Neuropathol. Exp. Neurol 69, 896–909 (2010). [PubMed: 20720507]
43. Pietrowski E et al. Pro-inflammatory effects of interleukin-17a on vascular smooth muscle cells involve NAD(P)H-oxidase derived reactive oxygen species. J. Vasc. Res 48, 52–58 (2011). [PubMed: 20606471]
44. Alves de Lima K et al. Meningeal γδ T cells regulate anxiety-like behavior via IL-17a signaling in neurons. Nat. Immunol 21, 1421–1429 (2020). [PubMed: 32929273]
45. Ribeiro M et al. Meningeal γδ T cell-derived IL-17 controls synaptic plasticity and short-term memory. Sci. Immunol 4, eaay5199 (2019). [PubMed: 31604844]
46. Rustenhoven J et al. Functional characterization of the dural sinuses as a neuroimmune interface. Cell 184, 1000–1016.e1027 (2021). [PubMed: 33508229]
47. Ranieri E, Netti GS & Gigante M CTL ELISPOT assay and T cell detection. Methods Mol. Biol 2325, 65–77 (2021). [PubMed: 34053051]
48. Jones HE, Abrams KA & Siegenthaler JA Techniques for visualizing fibroblast-vessel interactions in the developing and adult CNS. Neurophotonics 9, 021911 (2022). [PubMed: 35402637]
49. Derk J et al. Formation and function of the meningeal arachnoid barrier around the developing mouse brain. Dev. Cell 58, 635–644.e4 (2023). [PubMed: 36996816]
50. Zhang Y et al. Mucosal-associated invariant T cells restrict reactive oxidative damage and preserve meningeal barrier integrity and cognitive function. Nat. Immunol 23, 1714–1725 (2022). [PubMed: 36411380]
51. Prinz I, Silva-Santos B & Pennington DJ Functional development of γδ T cells. Eur. J. Immunol 43, 1988–1994 (2013). [PubMed: 23928962]
52. Gray EE et al. Deficiency in IL-17-committed vγ4^{+} γδ T cells in a spontaneous Sox13-mutant CD45.1^{+} congenic mouse substrain provides protection from dermatitis. Nat. Immunol 14, 584–592 (2013). [PubMed: 23624556]
53. McKenzie DR et al. lL-17-producing γδ T cells switch migratory patterns between resting and activated states. Nat. Commun 8, 15632 (2017). [PubMed: 28580944]
54. Mandala S et al. Alteration of lymphocyte trafficking by sphingosine-1-phosphate receptor agonists. Science 296, 346–349 (2002). [PubMed: 11923495]
55. Chiba K et al. FTY720, a novel immunosuppressant, induces sequestration of circulating mature lymphocytes by acceleration of lymphocyte homing in rats. J. Immunol 160, 5037–5044 (1998). [PubMed: 9590253]
56. Enosawa S, Suzuki S, Kakefuda T, Li XK & Amemiya H Induction of selective cell death targeting on mature T-lymphocytes in rats by a novel immunosuppressant, FTY720. Immunopharmacology 34, 171–179 (1996). [PubMed: 8886861]
57. Krebs CF et al. Autoimmune renal disease is exacerbated by S1P-receptor-1-dependent intestinal Th17 cell migration to the kidney. Immunity 45, 1078–1092 (2016). [PubMed: 27851911]
58. De Silva TM, Modrick ML, Grobe JL & Faraci FM Activation of the central renin-angiotensin system causes local cerebrovascular dysfunction. Stroke 52, 2404–2413 (2021). [PubMed: 34107734]
59. Lu X & Crowley SD The immune system in hypertension: a Lost Shaker of Salt 2021 Lewis K. Dahl Memorial Lecture. Hypertension 79, 1339–1347 (2022). [PubMed: 35545942]
60. Norlander AE, Madhur MS & Harrison DG The immunology of hypertension. J. Exp. Med 215, 21–33 (2018). [PubMed: 29247045]

61. Drummond GR, Vinh A, Guzik TJ & Sobey CG Immune mechanisms of hypertension. Nat. Rev. Immunol 19, 517–532 (2019). [PubMed: 30992524]
62. Higaki A, Mahmoud AUM, Paradis P & Schiffrin EL Role of interleukin-23/interleukin-17 axis in T-cell mediated actions in hypertension. Cardiovasc Res. 117, 1274–1283 (2020).
63. Louveau A et al. CNS lymphatic drainage and neuroinflammation are regulated by meningeal lymphatic vasculature. Nat. Neurosci 21, 1380–1391 (2018). [PubMed: 30224810]
64. Gorelick PB et al. Vascular contributions to cognitive impairment and dementia: a statement for healthcare professionals from the American Heart Association/American Stroke Association. Stroke 42, 2672–2713 (2011). [PubMed: 21778438]
65. Cortes-Canteli M & Iadecola C Alzheimer's disease and vascular aging: JACC focus seminar. J. Am. Coll. Cardiol 75, 942–951 (2020). [PubMed: 32130930]
66. Brigas HC et al. IL-17 triggers the onset of cognitive and synaptic deficits in early stages of Alzheimer's disease. Cell Rep. 36, 109574 (2021). [PubMed: 34469732]
67. Rouch L et al. Antihypertensive drugs, prevention of cognitive decline and dementia: a systematic review of observational studies, randomized controlled trials and meta-analyses, with discussion of potential mechanisms. CNS Drugs 29, 113–130 (2015). [PubMed: 25700645]
68. Ding J et al. Antihypertensive medications and risk for incident dementia and Alzheimer's disease: a meta-analysis of individual participant data from prospective cohort studies. Lancet Neurol. 19, 61–70 (2020). [PubMed: 31706889]
69. James PA et al. 2014 evidence-based guideline for the management of high blood pressure in adults: report from the panel members appointed to the Eighth Joint National Committee (JNC 8). JAMA 311, 507–520 (2014). [PubMed: 24352797]
70. Harrison DG, Coffman TM & Wilcox CS Pathophysiology of hypertension: the mosaic theory and beyond. Circ. Res 128, 847–863 (2021). [PubMed: 33793328]
71. Ridker PM et al. Antiinflammatory therapy with canakinumab for atherosclerotic disease. N. Engl. J. Med 377, 1119–1131 (2017). [PubMed: 28845751]
72. Ma T, Wang F, Xu S & Huang JH Meningeal immunity: structure, function and a potential therapeutic target of neurodegenerative diseases. Brain Behav. Immun 93, 264–276 (2021). [PubMed: 33548498]
73. Hayashi S, Lewis P, Pevny L & McMahon AP Efficient gene modulation in mouse epiblast using a Sox2Cre transgenic mouse strain. Mech. Dev 119, S97–S101 (2002). [PubMed: 14516668]
74. Belanger KM et al. Greater T regulatory cells in females attenuate DOCA-salt-induced increases in blood pressure versus males. Hypertension 75, 1615–1623 (2020). [PubMed: 32336228]
75. Korvela M et al. Quantification of 10 elements in human cerebrospinal fluid from chronic pain patients with and without spinal cord stimulation. J. Trace Elem. Med. Biol 37, 1–7 (2016). [PubMed: 27473826]
76. Bischoff K, Lamm C, Erb HN & Hillebrandt JR The effects of formalin fixation and tissue embedding of bovine liver on copper, iron, and zinc analysis. J. Vet. Diagn. Invest 20, 220–224 (2008). [PubMed: 18319437]
77. Capone C et al. The cerebrovascular dysfunction induced by slow pressor doses of angiotensin ii precedes the development of hypertension. Am. J. Physiol. Heart Circ. Physiol 300, H397–H407 (2011). [PubMed: 20971763]
78. Kober F et al. High-resolution myocardial perfusion mapping in small animals in vivo by spin-labeling gradient-echo imaging. Magn. Reson. Med 51, 62–67 (2004). [PubMed: 14705046]
79. Deacon RM Assessing nest building in mice. Nat. Protoc 1, 1117–1119 (2006). [PubMed: 17406392]
80. Faraco G et al. Dietary salt promotes cognitive impairment through tau phosphorylation. Nature 574, 686–690 (2019). [PubMed: 31645758]
81. Brea D et al. Stroke affects intestinal immune cell trafficking to the central nervous system. Brain Behav. Immun 96, 295–302 (2021). [PubMed: 33989742]
82. Louveau A, Filiano A & Kipnis J Meningeal whole mount preparation and characterization of neural cells by flow cytometry. Curr. Protoc. Immunol 121, e50 (2018). [PubMed: 30008983]

83. Goldmann T et al. Origin, fate and dynamics of macrophages at central nervous system interfaces. Nat. Immunol 17, 797–805 (2016). [PubMed: 27135602]
84. Borst K & Prinz M Deciphering the heterogeneity of myeloid cells during neuroinflammation in the single-cell era. Brain Pathol. 30, 1192–1207 (2020). [PubMed: 33058309]
85. Mendes NF & Velloso LA Perivascular macrophages in high-fat diet-induced hypothalamic inflammation. J. Neuroinflamm 19, 136 (2022).
86. Park L et al. Scavenger receptor CD36 is essential for the cerebrovascular oxidative stress and neurovascular dysfunction induced by amyloid-beta. Proc. Natl Acad. Sci. USA 108, 5063–5068 (2011). [PubMed: 21383152]
87. Rudick RA, Zirretta DK & Herndon RM Clearance of albumin from mouse subarachnoid space: a measure of CSF bulk flow. J. Neurosci. Methods 6, 253–259 (1982). [PubMed: 7144238]
88. Lim NK et al. An improved method for collection of cerebrospinal fluid from anesthetized mice. J. Vis. Exp 19, 56774 (2018).
89. Nakamoto H et al. Angiotensin-(1–7) and nitric oxide interaction in renovascular hypertension. Hypertension 25, 796–802 (1995). [PubMed: 7536715]
90. Park L et al. Tau induces PSD95-neuronal nos uncoupling and neurovascular dysfunction independent of neurodegeneration. Nat. Neurosci 23, 1079–1089 (2020). [PubMed: 32778793]

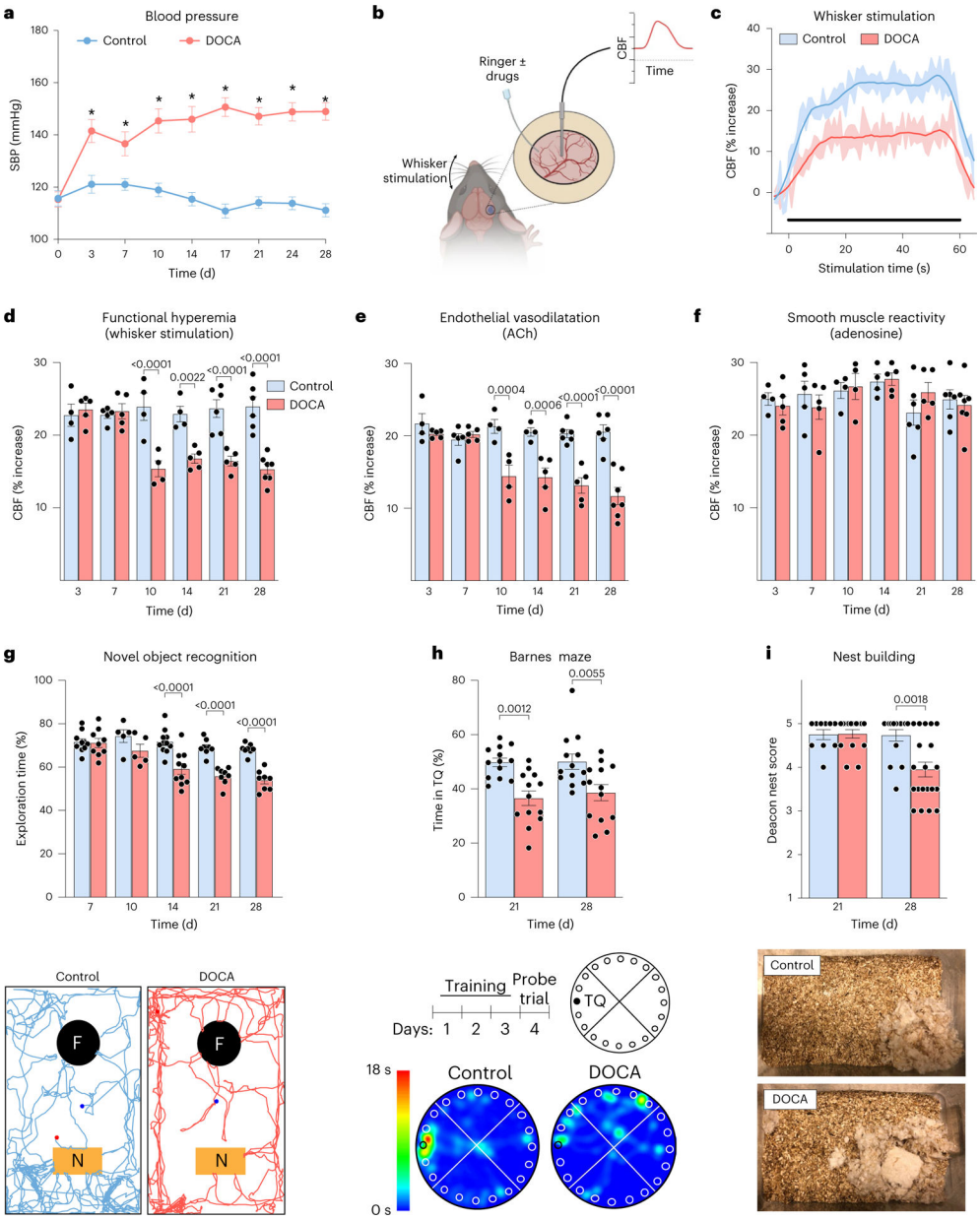

Fig. 1 |. DOCA-salt HTN induces neurovascular and cognitive impairment.

a, SBP, assessed by tail-cuff plethysmography, is elevated in DOCA-salt HTN over 28 days of treatment (HTN, $P < 0.0001$; time, $P < 0.0001$; interaction, $P < 0.0001$; $n = 15$ mice per group). **b**, Schematic of methods used to assess neurovascular function (created with BioRender.com). **c**,**d**, DOCA attenuates the increase in CBF induced by 60-s stimulation (**c**) of the facial whiskers (functional hyperemia), beginning at 10 d of DOCA (**d**) (HTN, $P < 0.0001$; time, $P = 0.001$; interaction, $P < 0.0001$; $n = 4$–7 mice per group as shown). **e**, Endothelial vasodilatation was attenuated by DOCA beginning at 10 d (HTN, $P < 0.0001$; time, $P < 0.0001$; interaction, $P < 0.0001$; $n = 4$–7 mice group as shown). **f**, No difference observed in smooth muscle reactivity (HTN, $P = 0.9702$; time, $P = 0.1981$; interaction, $P = 0.6479$; $n = 4$–7 mice per group as shown). **g**–**i**, DOCA-induced cognitive impairment

assessed by percentage time exploring a novel object (HTN, $P < 0.0001$; time, $P < 0.0001$; interaction, $P = 0.0012$; $n = 5–11$ mice per group as shown) (**g**), time in TQ during the Barnes maze probe trial (HTN, $P < 0.0001$; time, $P = 0.6531$; interaction, $P = 0.7123$; $n = 13$ mice per group) (**h**) and nest building assessed on the Deacon score scale (HTN, $P = 0.0125$; time, $P = 0.0069$; interaction, $P = 0093$; $n = 10–20$ mice per group as shown) (**i**). Representative images of a single mouse from each group are shown for novel object recognition, the Barnes maze probe trial and nest building. All intergroup differences are analyzed by two-way ANOVA and Bonferroni's multiplecomparison test. Data are shown as mean ± s.e.m.

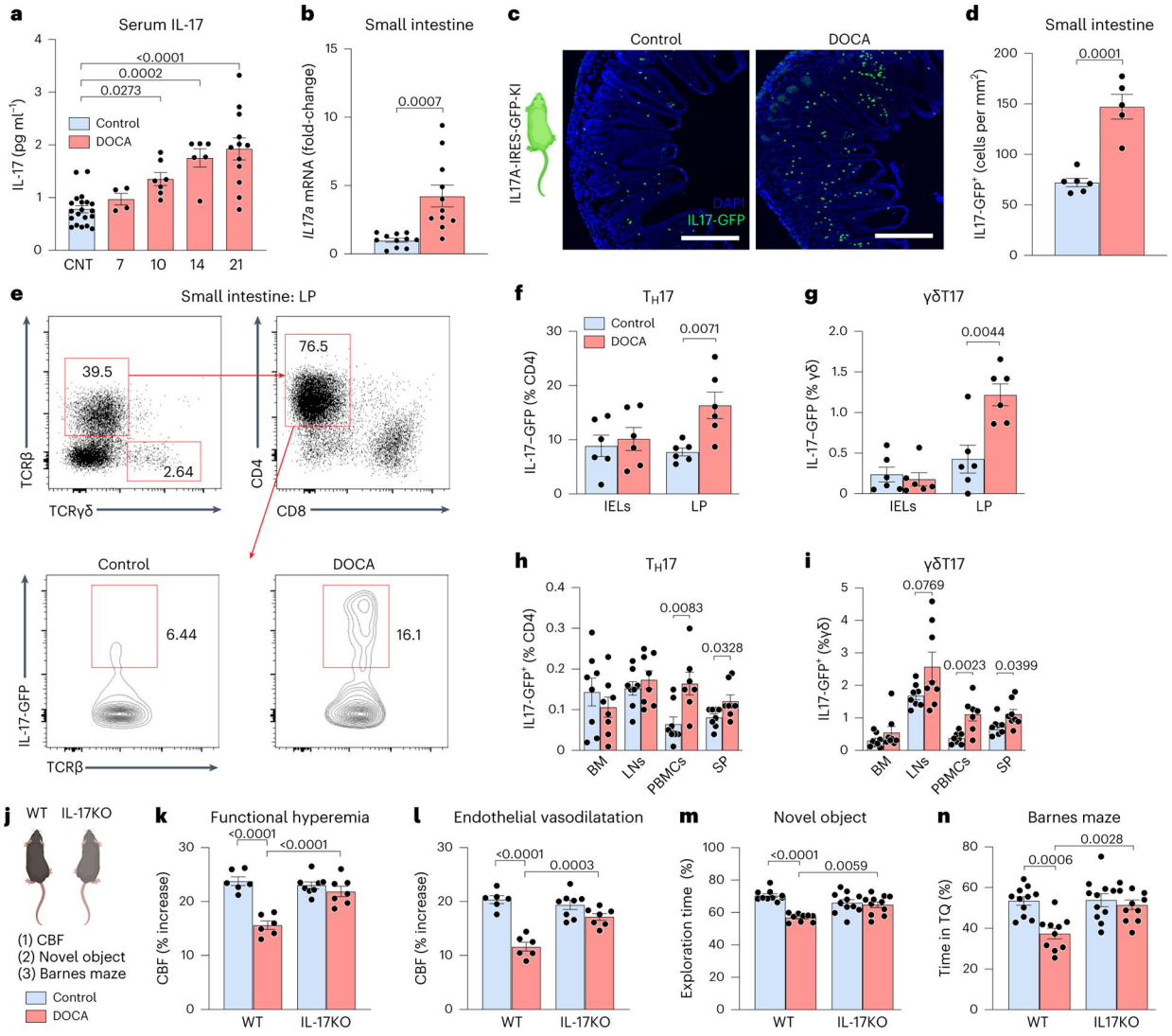

Fig. 2 |. The neurovascular and cognitive impairment induced by DOCA is mediated by IL-17.

a, Serum IL-17 elevated in DOCA HTN starting at 10 d ($P < 0.0001$; one-way ANOVA and Bonferroni's multiple-comparison test; $n = 5$–18 mice per group as shown). **b**, Then, 21 d of DOCA-salt increasing *Il17a* mRNA (unpaired, two-tailed Student's *t*-test, $n = 11$ mice per group). **c**, Representative images of IL-17-GFP cells in the small intestine of control and DOCA-salt. Scale bar, 300um. **d**, 21 d of DOCA-salt also increases IL-17-GFP cells in the small intestine (unpaired, two-tailed Student's *t*-test, $n = 5$ and 6 mice per group). **e**–**g**, Cells identified by flow cytometry as T_H17 cells (**f**) and γδT17c cells (**g**) in the lamina propria (LP) (**e**) not intraepithelial lymphocytes (unpaired, two-tailed Student's *t*-test, n = 6 mice per group). **h**,**i**, T_H17 cells (**h**) and γδT17 cells (**i**) also expanded in peripheral blood mononuclear cells (PBMCs) and spleen (SP), but not in the bone marrow or lymph nodes (LNs) (unpaired, two-tailed Student's *t*-test per organ, $n = 7$ and 8 mice per group). **j**–**n**, IL-17-deficient mice (KO) (**j**) not exhibiting an attenuation in functional hyperemia (HTN, $P < 0.0001$; genotype, $P = 0.0024$; interaction, $P = 0.0002$; two-way ANOVA and Bonferroni's multiple-comparison test; $n = 6$–8 mice per group as shown) (**k**), endothelial

vasodilatation (HTN, $P < 0.0001$; genotype, $P = 0.0079$; interaction, $P = 0.0004$; two-way ANOVA and Bonferroni's multiple-comparison test; $n = 6–8$) (**l**) and no deficits observed in either novel object recognition (HTN, $P < 0.0001$; genotype, $P = 0.2603$; interaction, $P = 0.0003$; two-way ANOVA and Bonferroni's multiple-comparison test; $n = 9–11$ mice per group as shown) (**m**) or Barnes maze tests (HTN, $P = 0.0010$; genotype, $P = 0.0076$; interaction, $P = 0.0114$; two-way ANOVA and Bonferroni's multiple-comparison test; $n = 9–11$ mice per group as shown) (**n**). Data are shown as mean ± s.e.m. Schematics were created with BioRender.com.

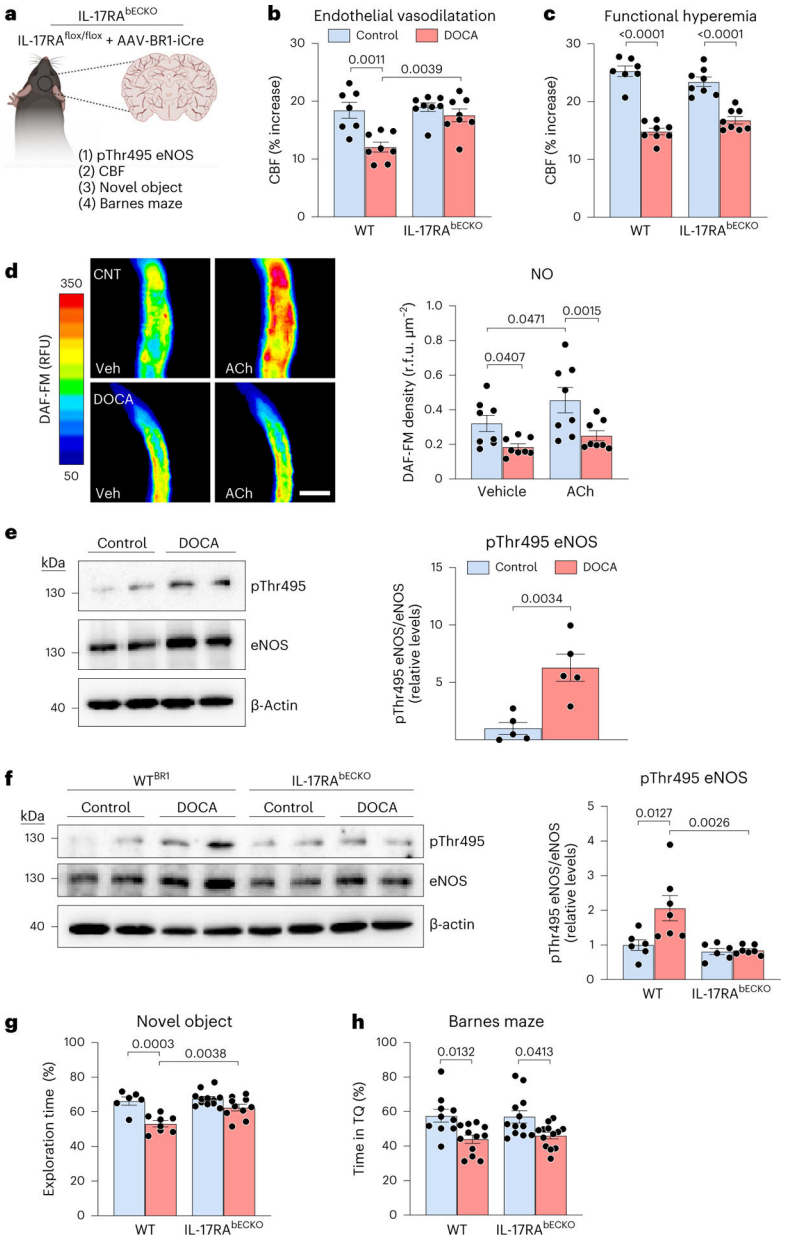

Fig. 3 |. IL-17 impairs endothelial vasodilatation by downregulating NO bioavailability via endothelial IL-17 receptors.

a–**c**, IL-17RA brain endothelial cell KO (IL-17RA^{bECKO}) mice (**a**) protected from impairment in endothelial vasodilatation (HTN, $P = 0.0007$; genotype, $P = 0.0067$; interaction, $P = 0.0223$; two-way ANOVA and Bonferroni's multiple-comparison test; $n = 7–8$ mice per group as shown) (**b**) but not impairment in functional hyperemia induced by DOCA (HTN, $P < 0.0001$; genotype, $P = 0.9446$; interaction, $P = 0.0161$; two-way ANOVA and Bonferroni's multiple-comparison test; $n = 7–8$ mice per group as shown) (**c**). **d**, Resting and ACh-induced endothelial NO production attenuated in DOCA cerebral microvascular preparations ($P < 0.0001$, repeated measured one-way ANOVA and Tukey's multiple-comparison test; $n = 8$ mice per group). Veh, Vehicle. Scale bar, 50 µm. **e**,**f**, eNOS inhibitory phosphorylation increased by DOCA in WT mice (unpaired, two-tailed Student's

t-test) (**e**), an effect suppressed in IL-17RA^{bECKO} mice (HTN, $P = 0.0185$; genotype, $P = 0.0037$; interaction, $P = 0.0266$; two-way ANOVA and Bonferroni's multiple-comparison test; $n = 5–7$ mice per group as shown) (**f**). **g**,**h**, IL-17RA^{bECKO} displayed cognitive improvement only in novel object recognition (HTN, $P < 0.0001$; genotype, $P = 0.0061$; interaction, $P = 0.0338$; two-way ANOVA and Tukey's multiplecomparison test; $n = 6–12$ mice per group as shown) (**g**), not the Barnes maze test (HTN, $P = 0.0001$; genotype, $P = 0.8102$; interaction, $P = 0.6488$; two-way ANOVA and Tukey's multiple-comparison test; $n = 10–13$ mice per group as shown) (**h**). Data are shown as mean ± s.e.m. Schematics created with BioRender.com.

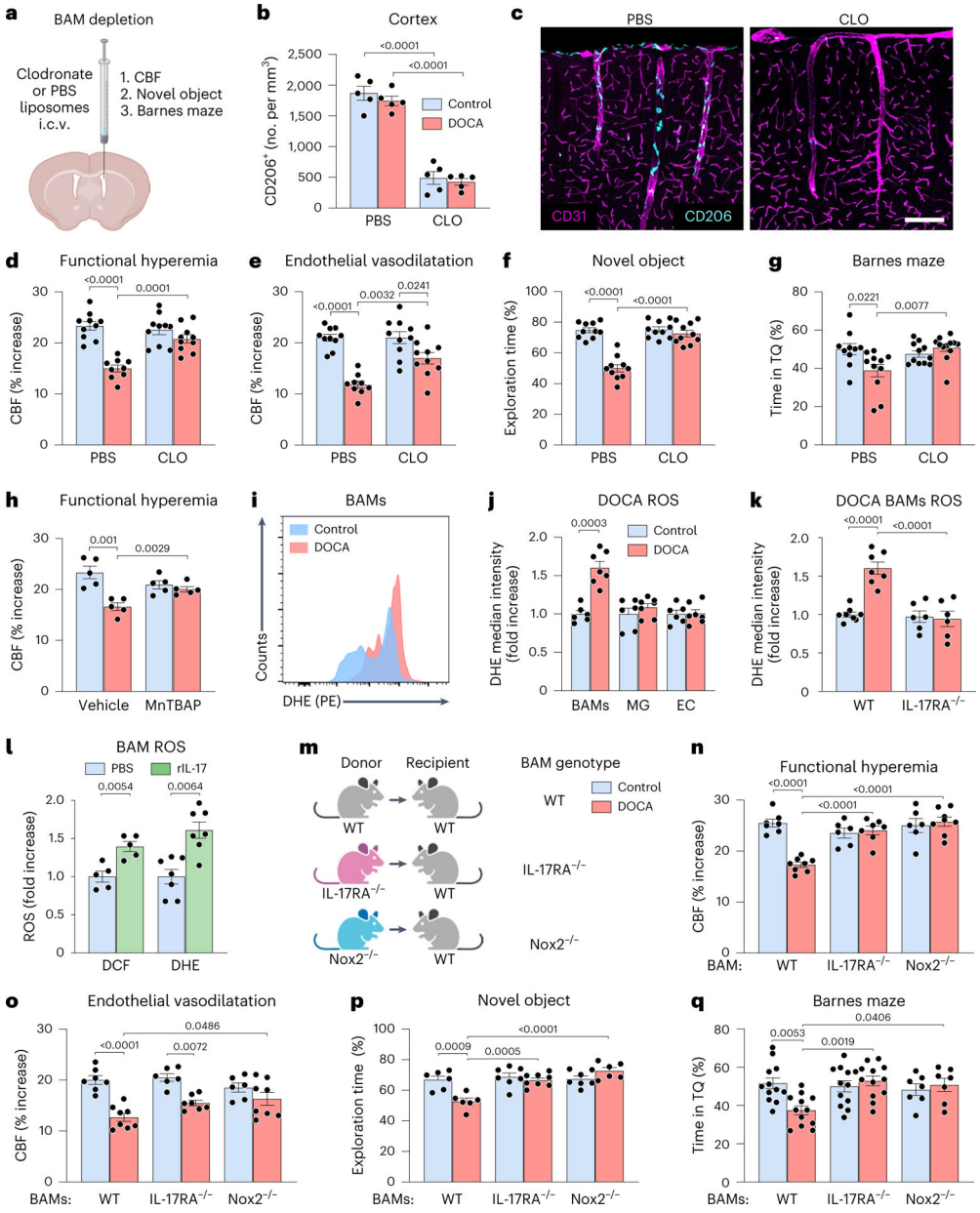

Fig. 4 |. IL-17 impairs functional hyperemia via enhanced ROS production mediated by IL-17RA in BAMs.

a,**b**, BAMs, including perivascular and leptomeningeal macrophages (**a**), depleted by 80% 21 d after delivery i.c.v. of liposome-encapsulated clodronate (CLO) depletion (**b**) (HTN, $P = 0.3156$; liposomes, $P < 0.0001$; interaction, $P = 0.7305$; two-way ANOVA and Tukey's multiple-comparison test; $n = 5$ mice per group). **c**, Representative images of CD206 BAMs in PBS and CLO treated mice. Scale bar, 150 μm. **d**–**g**, BAM depletion normalized functional hyperemia (HTN, $P < 0.0001$; liposomes, $P = 0.0050$; interaction, $P = 0.0004$; two-way ANOVA and Tukey's multiple-comparison test; $n = 9$–10 mice per group as shown) (**d**) and partially improved endothelial vasodilation (HTN, $P < 0.0001$, liposomes, $P = 0.0100$, interaction, $P = 0.0112$, two-way ANOVA and Tukey's multiple-comparison test; $n = 9$–10 mice per group as shown) (**e**) while also improving cognitive function assessed by

novel object recognition (HTN, $P < 0.0001$; liposomes, $P < 0.0001$; interaction, $P < 0.0001$; two-way ANOVA and Bonferroni's multiple-comparison test; $n = 10$ mice per group as shown) (**f**) and the Barnes maze test (HTN, $P = 0.1240$; liposomes, $P = 0.0648$; interaction, $P = 0.0062$, two-way ANOVA and Bonferroni's multiple-comparison test; $n = 10$–12 mice per group as shown) (**g**). **h**, Neocortical application of the ROS scavenger MnTBAP rescuing the impairment of functional hyperemia in DOCA-salt HTN ($P = 0.0090$; treatment, $P = 0.3418$; interaction, $P = 0.0005$, two-way repeated measures ANOVA with Bonferroni's multiple-comparison test; $n = 5$ mice per group). **i**–**k**, The increased ROS production in BAMs (**i**) induced by DOCA-salt (HTN, $P = 0.0033$; cell type, $P < 0.0001$, interaction, $P < 0.0001$; two-way repeated measures ANOVA with Bonferroni's multiple-comparison test; $n = 6$–7 mice per group as shown) (**j**) prevented in IL-17RA-deficient mice (HTN, $P = 0.0006$; genotype, $P < 0.0001$; interaction, $P = 0.0002$; two-way ANOVA with Bonferroni's multiple-comparison test; $n = 6$–8 mice per group as shown) (**k**). MG, microglia. EC, endothelial cells. **l**, Recombinant IL-17 increased ROS production in BAMs (paired, two-tailed Student's *t*-test per ROS indicator; $n = 5$–8 biological replicates). **m**–**q**, Deletion of either IL-17RA or Nox2 from BAM in BM chimeras (**m**) preventing the impairment of functional hyperemia in full (HTN, $P = 0.0030$; BAM genotype, $P = 0.0003$; interaction, $P < 0.0001$; two-way ANOVA with Tukey's multiple-comparison test; $n = 6$–8 mice per group as shown) (**n**), improved endothelial vasodilation (HTN, $P < 0.0001$; BAM genotype, $P = 0.1898$; interaction, $P = 0.0248$; two-way ANOVA with Tukey's multiple-comparison test; $n = 6$–8 mice per group as shown) (**o**), as well as cognitive function (novel object (**p**): HTN, $P = 0.0392$, BAM genotype, $P < 0.0001$; interaction, $P = 0.0004$ or the Barnes maze test (**q**): HTN, $P = 0.2287$; BAM genotype, $P = 0.0362$; interaction, $P = 0.0040$; two-way ANOVA with Tukey's multiple-comparison test; $n = 7$–12 mice per group as shown). Data are shown as mean ± s.e.m. Schematics created with BioRender.com.

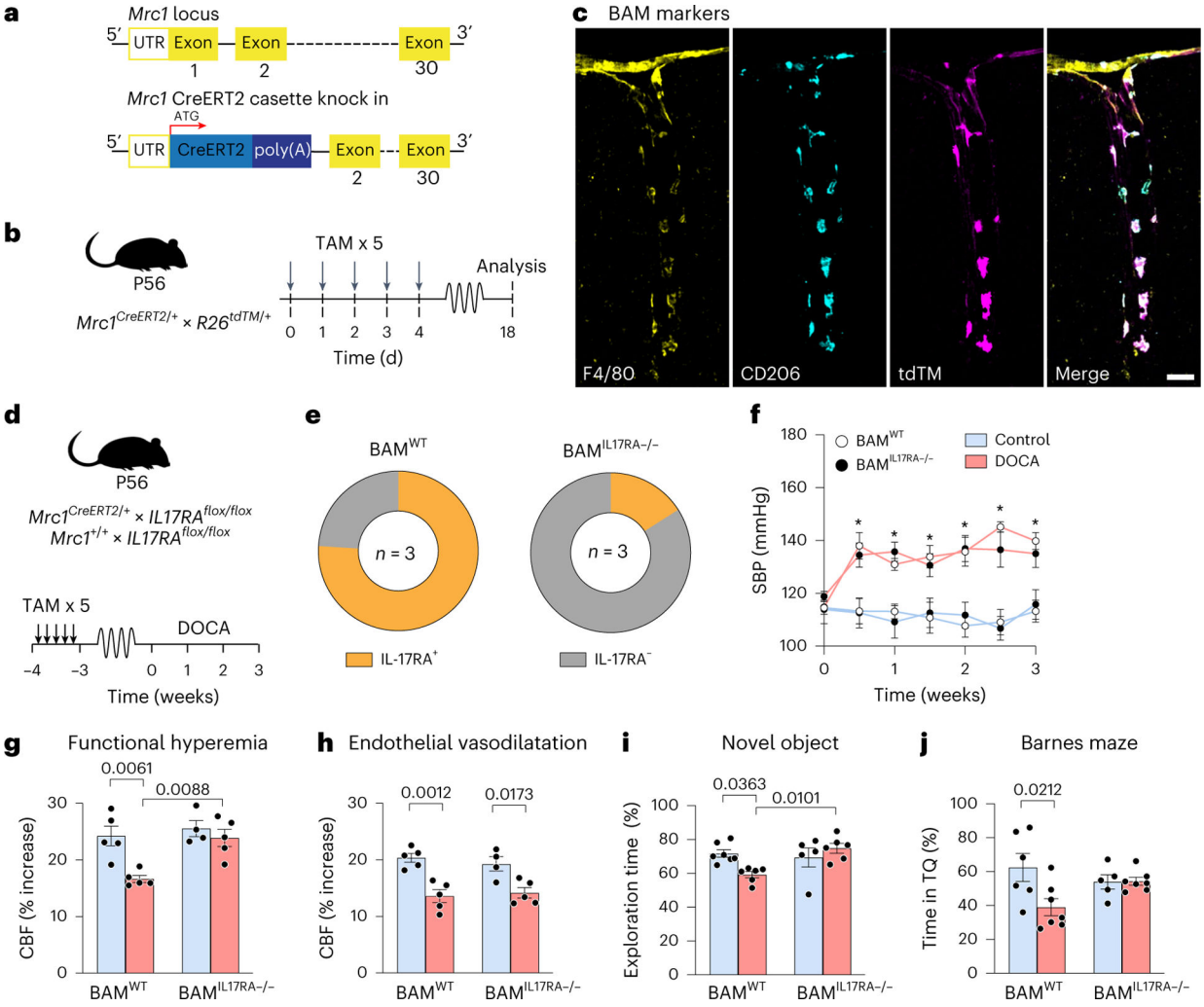

Fig. 5 |. IL-17RA deletion in BAMs improves functional hyperemia and cognitive function in DOCA-salt.

a, CreERT2 cassette introduced into the endogenous Mrc1 locus. **b**, Mrc1CreERT2 mice crossed with the Ai14 TdTomato reporter mice. **c**, TdTM expression in BAMs (experiment repeated three times). Scale bar, 50 μm. **d**, $Mrc1^{CreERT2}$ mice crossed with IL-17RA$^{flox/flox}$ to generate $BAM^{IL17RA-/-}$. **e**, IL-17RA expression reduced by 78.9% in $BAM^{IL17RA-/-}$ compared with BAM^{WT} mice ($n = 3$ mice per group; 50 BAMs per mouse; interaction IL-17RA expression × genotype, $P < 0.0001$, two-way repeated measures ANOVA with Bonferroni's multiple-comparison test). **f**, BP under control and DOCA-salt conditions not altered in BAM^{WT} or $BAM^{IL17RA-/-}$ mice ($n = 5$–7 mice per group; experimental group, $P < 0.0001$; time, $P = 0.0050$; interaction, $P = 0.0018$; two-way repeated measures ANOVA with Tukey's multiple-comparison test). **g**,**h**, IL-17RA deletion in BAMs restoring functional hyperemia (HTN, $P = 0.0048$; genotype, $P = 0.0080$; interaction, $P = 0.0499$; two-way ANOVA with Bonferroni's multiple-comparison test; $n = 4$–5 mice per group as shown) (**g**) without improving endothelial vasodilatation (HTN, $P < 0.001$; genotype, $P = 0.8120$; interaction, $P = 0.4368$; two-way ANOVA with Tukey's multiple-comparison test; $n = 4$–5 mice per group as shown) (**h**). **i**,**j**, Rescued cognitive function after 21 d of DOCA-salt

(novel object (**i**): HTN, $P = 0.2638$; genotype, $P = 0.0460$; interaction, $P = 0.0100$); Barnes maze test (**j**): HTN, $P = 0.0427$; genotype, $P = 0.5297$; interaction, $P = 0.0365$; two-way ANOVA with Tukey's multiple-comparison test; n = 5–7 mice per group as shown). Data are shown as mean ± s.e.m.

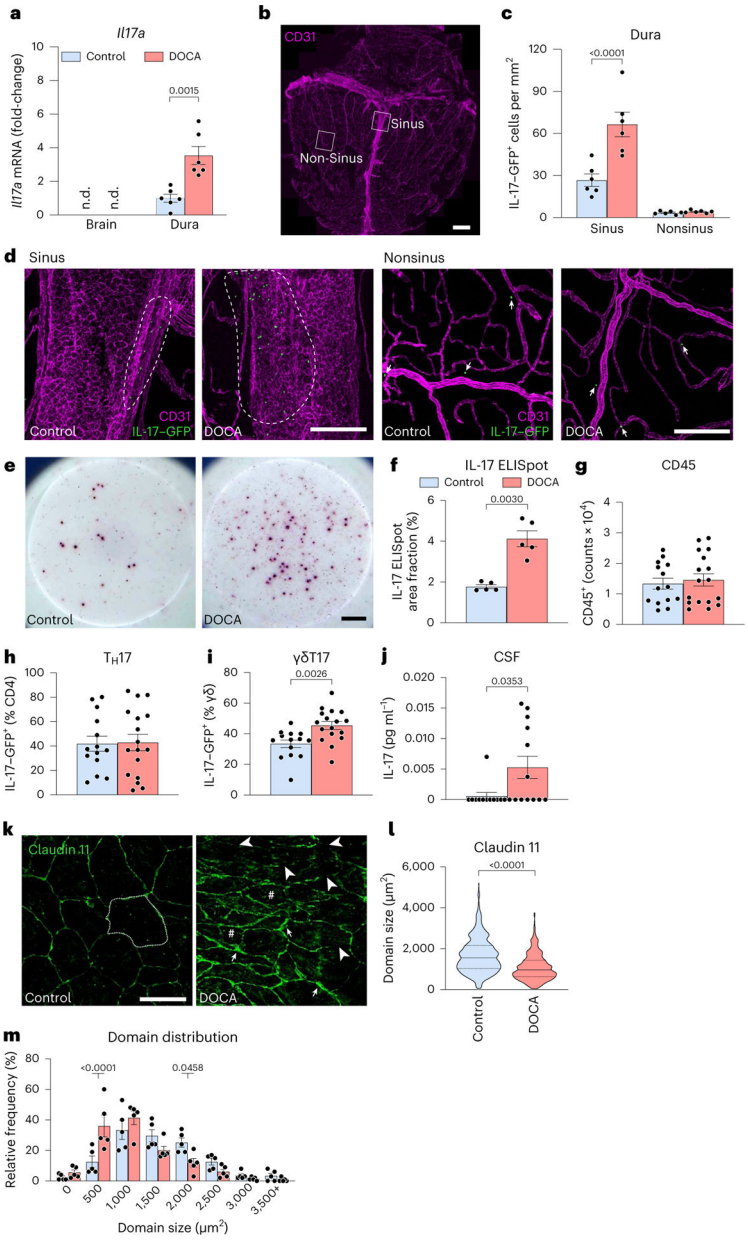

Fig. 6 |. Salt-sensitive hypertension increases IL-17-producing T cells located in the dura mater. **a**, *Il17a* mRNA not observed in the brain, but detected in dura mater of control mice and markedly increased by DOCA-salt (unpaired, two-tailed Student's *t*-test; $n = 6$). **b**, Dura whole mount stained with CD31 (magenta). Scale bar, 1 mm. **c**, DOCA-salt treatment leading to a significant increase in IL-17–GFP$^+$ cells surrounding the venous sinuses (HTN, $P = 0.0017$; sinus, $P < 0.0001$; interaction, $P = 0.0034$; two-way repeated measures ANOVA with Bonferroni's multiple-comparison test; $n = 6$ mice per group). **d**, Representative images of control and DOCA sinus and nonsinus regions. Scale bar, 200 μm. Analysis is shown in **c**. **e**,**f**, Dural isolated cells secreting IL-17 (**e**), a response increased in DOCA-salt mice (unpaired, two-tailed Student's *t*-test with Welch's correction; $n = 5$ mice per group) (**f**). Scale bar, 1 mm. **g**, DOCA-salt not changing the total number of CD45 immune cells

isolated from dura (unpaired, two-tailed Student's *t*-test; control $n = 14$, DOCA $n = 17$ mice per group as shown). **h**,**i**, DOCA-salt increasing the percentage of γδT17 cells but no difference in T_H17 cells (unpaired, two-tailed Student's *t*-test; control (**h**) $n = 14$, DOCA (**i**) $n = 17$ mice per group as shown). **j**, IL-17 detection increased in the CSF after 21 d of DOCA-salt (two-tailed Mann–Whitney *U*-test, control $n = 12$, DOCA $n = 13$ mice). **k**, Arachnoid barrier integrity was assessed by the arachnoid barrier tight junction marker claudin-11. Arrowheads indicate discontinuous tight junctions, # indicates reduced arachnoid domain size and thin arrows indicate altered tight junction morphology. Scale bar, 50 μm. **l**,**m**, Arachnoid barrier domain size (Kolmogrov–Smirnov test; control $n = 663$ domains, DOCA $n = 616$ domains (5 mice, 10 images per mouse, all domains per image quantified) (**l**), lines in violin plot indicate median and quartiles) and distribution was altered by DOCA-salt (HTN, $P = 0.9880$; domain size bin, $P < 0.0001$; interaction, $P < 0.0001$; two-way ANOVA with Bonferroni's multiple-comparison test) (**m**). Data are shown as mean ± s.e.m.

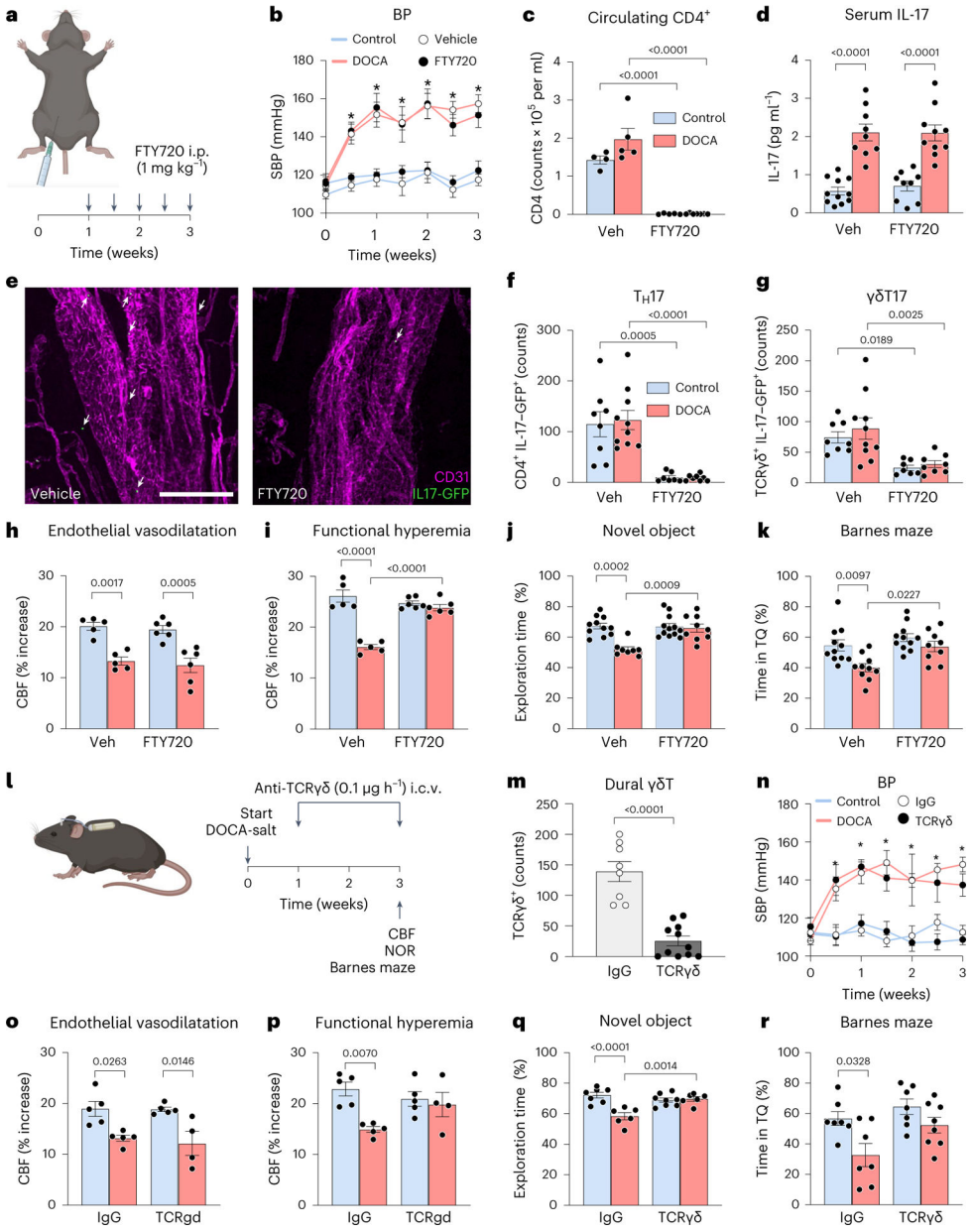

Fig. 7 |. Cognitive impairment in salt-sensitive HTN is driven by meningeal IL-17-producing T cells.

a,**b**, FTY720 administered from day 7 to day 21 (**a**) of DOCA-salt not affecting the increase in SBP (**b**) (treatment, $P < 0.0001$; time, $P < 0.0001$; interaction, $P = 0.0105$; two-way repeated measures ANOVA with Tukey's multiple-comparison test; $n = 5$–7 mice per group). **c**,**d**, FTY720 reducing circulating CD4 T cells (HTN, $P = 0.0705$; treatment, $P < 0.0001$; interaction, $P = 0.0737$; two-way ANOVA with Tukey's multiple-comparison test; $n = 4$–7 mice per group as shown) (**c**), without affecting the elevation in serum IL-17 in DOCA-salt (HTN, $P < 0.0001$; treatment, $P = 0.7200$; interaction, $P = 0.6622$; two-way ANOVA with Tukey's multiple-comparison test; $n = 9$–11 mice per group as shown) (**d**). **e**–**g**, FTY720 reducing IL-17–GFP cells (**e**) in the dura, including both T_H17 cells (HTN, $P = 0.8358$; treatment, $P < 0.0001$; interaction, $P = 0.7848$; two-way ANOVA with Bonferroni's

multiple-comparison test; n = 7–10 mice per group as shown) (**f**) and γδT17 cells (HTN, P = 0.4044; treatment, P = 0.0001; interaction, P = 0.7150; two-way ANOVA with Bonferroni's multiple-comparison test; n = 7–10 mice per group as shown) (**g**). **h**–**k**, FTY720 did not improve endothelial vasodilation (HTN, P < 0.0001; treatment, P = 0.4839; interaction, P = 0.9293; two-way ANOVA with Bonferroni's multiple-comparison test; vehicle n = 5, FTY720 n = 6 mice per group) (**h**), but completely restored functional hyperemia (HTN, P < 0.0001; treatment, P = 0.0004; interaction, P < 0.0001; two-way ANOVA with Bonferroni's multiple-comparison test; vehicle, n = 5, FTY720, n = 6 mice) (**i**), as well as improved cognitive function (novel object (**j**): HTN, P = 0.0007; treatment, P = 0.0037; interaction, P = 0.0023; Barnes maze test (**k**): HTN, P = 0.0023; treatment, P = 0.0045; interaction, P = 0.1695; two-way ANOVA with Tukey's multiple-comparison test; n = 8–12 mice per group as shown). **l**, Anti-TCRγδ antibody delivered i.c.v. from day 7 to day 21 of DOCA-salt. **m**, Anti-TCRγδ antibody treatment reducing γδT cells in the dura (two-tailed, unpaired Student's t-test, n = 8–11 mice per group as shown). **n**, Anti-TCRgd antibody not altering the BP response to DOCA-salt (HTN, P < 0.0001; time, P < 0.0001; interaction, P = 0.0016; two-way repeated measures ANOVA with Tukey's multiple-comparison test; n = 5–6 mice per group). **o**–**r**, Dural γδT cell depletion did not restore endothelial vasodilatation (HTN, P = 0.0001; treatment, P = 0.6673; interaction, P = 0.7281; two-way ANOVA with Tukey's multiple-comparison test; n = 4–5 mice per group as shown) (**o**), but was associated with improved functional hyperemia (HTN, P = 0.0082; treatment, P = 0.3407; interaction, P = 0.0365; two-way ANOVA with Tukey's multiple-comparison test; n = 4–5 mice per group as shown) (**p**) and cognitive function (novel object (**q**): HTN, P = 0.0012; treatment, P = 0.0323; interaction, P = 0.0004; Barnes maze (**r**): HTN, P = 0.0040; treatment, P = 0.0229; interaction, P = 0.3002; two-way ANOVA with Tukey's multiple-comparison test; n = 6–8 mice per group as shown). Data are shown as mean ± s.e.m. Schematics created with BioRender.com.

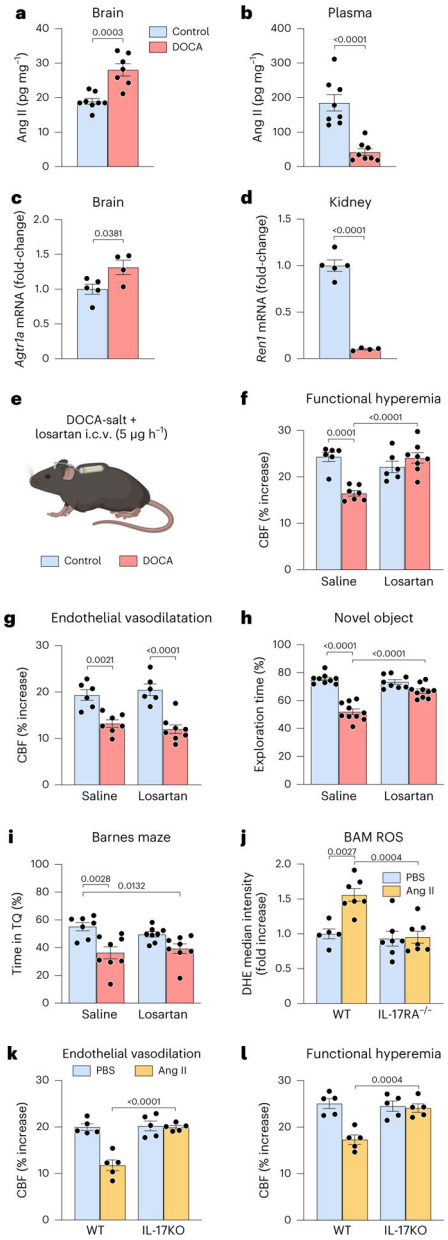

Fig. 8 |. The contribution of Ang II to the cerebrovascular dysfunction in DOCA-salt depends on IL-17 signaling.

a,**b**, DOCA-salt treatment elevating Ang II levels in brain (**a**) and reducing it in the circulation (**b**) (unpaired, two-tailed Student's *t*-test; $n = 7–8$ mice per group as shown). **c**,**d**, DOCA-salt upregulating brain *Agtr1a* (**c**) and downregulating kidney renin (**d**) (unpaired, two-tailed Student's *t*-test; $n = 4–5$ mice per group as shown). **e**–**g**, Central AT1R blockade with chronic losartan i.c.v. (**e**) restoring functional hyperemia (HTN, $P = 0.0088$; treatment, $P = 0.0148$; interaction, $P < 0.0001$; two-way ANOVA with Bonferroni's multiple-comparison test; $n = 6–8$ mice per group as shown) (**f**), but not improving endothelium-dependent vasodilatation (HTN, $P < 0.0001$; treatment, $P = 0.9604$; interaction, $P = 0.2642$; two-way ANOVA with Bonferroni's multiple-comparison test; $n = 6–8$ mice

per group as shown) (**g**). **h**,**i**, Central AT1R blockade improving novel object recognition (HTN, $P < 0.0001$; treatment, $P = 0.0005$; interaction, $P < 0.0001$; two-way ANOVA with Bonferroni's multiple-comparison test; $n = 8–10$ mice per group as shown) (**h**), but not improving Barnes maze test (HTN, $P = 0.0002$; treatment, $P = 0.6968$; interaction, $P = 0.2113$; two-way ANOVA with Tukey's multiple-comparison test; $n = 7–8$ mice per group as shown) (**i**). **j**, Ang II stimulation increasing ROS production in WT but not IL-17RA$^{-/-}$ BAMs (genotype, $P = 0.0015$; treatment, $P = 0.0050$; interaction, $P = 0.0087$; two-way ANOVA with Tukey's multiple-comparison test; $n = 5–7$ biological replicates per group as shown). **k**,**l**, Neocortical application of Ang II impairing endothelial vasodilation (genotype, $P = 0.0029$; treatment, $P = 0.0003$; interaction, $P = 0.0004$; two-way repeated measures ANOVA with Bonferroni's multiple-comparison test; $n = 5$ mice per group) (**k**) and inducing neurovascular dysfunction (genotype, $P = 0.0374$; treatment, $P = 0.0003$; interaction, $P = 0.0005$; two-way repeated measures ANOVA with Bonferroni's multiple-comparison test; $n = 5$ mice per group) (**l**) in WT but not IL-17KO mice. Data are shown as mean ± s.e.m. Schematics created with BioRender.com.